

MORPHEUS: BENCHMARKING PHYSICAL REASONING OF VIDEO GENERATIVE MODELS WITH REAL PHYSICAL EXPERIMENTS

Chenyu Zhang^{1,*}, Daniil Cherniavskii^{2,*}, Andrii Zadaianchuk^{2,*}, Antonios Tragoudaras^{2,*}, Antonios Vozikis^{2,†}, Thijmen Nijdam^{2,†}, Derck W. E. Prinzhorn², Mark Bodracska², Nicu Sebe¹, and Efstratios Gavves^{2,3}

¹University of Trento, Italy

²University of Amsterdam, the Netherlands

³Archimedes, Athena Research Center, Greece

ABSTRACT

Recent advances in image and video generation raise hopes that these models possess world modeling capabilities—the ability to generate realistic, physically plausible videos. This could revolutionize applications in robotics, autonomous driving, and scientific simulation. However, before treating these models as world models, we must ask: Do they adhere to physical conservation laws? To answer this, we introduce **Morpheus**, a benchmark for evaluating video generation models on physical reasoning. It features 80 real-world videos capturing physical phenomena, guided by conservation laws. Since artificial generations lack ground truth, we assess physical plausibility using physics-informed metrics evaluated with respect to infallible conservation laws known per physical setting, leveraging advances in physics-informed neural networks and vision-language foundation models. Our findings reveal that even with advanced prompting and video conditioning, current models struggle to encode physical principles despite generating aesthetically pleasing videos. All data, leaderboard, and code are open-sourced at: <https://physics-from-video.github.io/morpheus-bench/>

1 Introduction

Video generative models (VGMs) such as SORA [7], Veo2 [8], and COSMOS [5] have taken the world by storm, building upon remarkable advances in image generative models [9, 10, 11, 12], and achieving unprecedented levels of visual fidelity and realism.

These developments have not only pushed the boundaries of visual aesthetics but have also inspired the community to envision video generative models as potential *world models* [13, 5]. A world model, in this context, is more than just a system for generating frames, however; it is a model capable of understanding and predicting the dynamics, causal interactions, and underlying mechanisms of the physical world. Accurately benchmarking the physical dynamics of video generation is a critical requirement—and the focus of this work—toward adopting them potentially as world models.

Evaluating physical dynamics of generated video is far from straightforward. When describing physical systems,

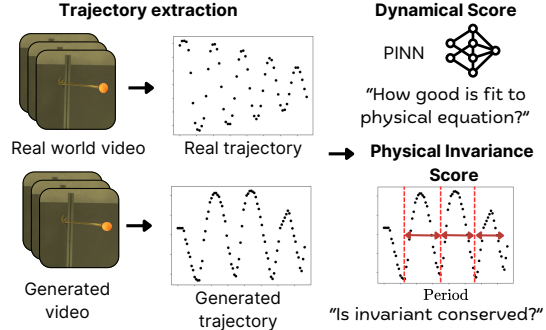


Figure 1: Physical Evaluation of VGMs for the holonomic pendulum experiment using Dynamical and Physical Invariance scores computed from the extracted trajectories.

the mathematical descriptions such as Hamiltonians or Lagrangians correspond to idealized and simplified setups¹.

For instance, we often approximate objects to be point

*denotes equal first author contribution

†denotes equal second author contribution

Benchmark	Real-world ground-through	Quantitative evaluation	Initial condition grounding	Physical laws evaluation
VideoCon-Physics [1]	✓	✗	✗ (only text)	✗
VAMP [2]	✓	✓	✗ (only text)	✗
PhyGenBench [3]	✓	✗	✗ (only text)	✗
Kang et al. [4]	✗	✓	✓ (1 or 3 frames)	✗
COSMOS [5]	✗	✓	✓ (image and video)	✗
Physics-IQ [6]	✓	✓	✓ (image and video)	✗
Morpheus (ours)	✓	✓	✓ (image and video)	✓

Table 1: Comparison of physics-based video understanding benchmarks. Symbols: ✓ = supported, ✗ = not supported

masses for convenience or we assume perfect knowledge of physical variables such as velocity or acceleration. Evaluating the physics in generated videos, however, refers to the exact opposite setting: assessing to what extent the physics of arbitrary—not stylized—videos, featuring arbitrarily shaped objects and non-canonical viewing angles, are preserved in terms of the *Ordinary Differential Equation (ODE) dynamics* governing the underlying physical system. Evaluating the plausibility of these ODE dynamics in governing the generated pixels is key to assessing the physical plausibility of the video. Perhaps the most daring challenge from an AI perspective, however, is that physical dynamics evaluation go beyond visual verification, whether in terms of a) spatiotemporal locations of objects (e.g., predicting the future location of a projectile correctly) [4, 6], b) human judgement (e.g., “does this video of an object falling look legitimate?”) [1, 3], or c) visual plausibility (e.g., “is the generated object visually consistent through time?”) [5]. A deeper physical understanding requires accurately capturing the *physical invariants* that govern these systems, that is, system properties such as total energy of a system, that remain consistent as it evolves, providing opportunities for both qualitative and quantitative benchmarks for physical reasoning. Using these invariants, we can design systematic benchmarks that reveal whether video generative models truly understand the dynamics of the physical world or simply create visually plausible approximations.

We propose **Morpheus**, a novel benchmarking framework designed to evaluate the physical reasoning capabilities of video generative models using real-world physical experiments. The key idea behind **Morpheus** is to map video recordings of physical events—whether generated by models or recorded from real experiments—into a common physical representation that can be analyzed and compared. Leveraging advances in zero-shot object segmentation, object tracking, and physics-informed neural networks (PINNs) [14, 15], our framework a) fits to the video dynamics the ODE dynamics that should be governing the underlying system, and b) extracts standardized physical measurements, such as velocity and acceleration from video data, which should conform to conservation laws. By collecting measurements from both real physical videos and generated ones, and comparing their summary statistics with respect to governing ODEs and physical invariants, **Morpheus** enables fair and systematic benchmarking of

physical invariants, such as the conservation of energy or momentum, without requiring explicit ground truth data.

We make four contributions toward benchmarking the physical reasoning capabilities of video generative models.

First, we introduce **Morpheus**, the first benchmark, including a public leaderboard, using real-world physical experiments to systematically evaluate physical reasoning based explicitly on physical invariants (section 3).

Second, we propose a novel framework that combines physics-informed deep learning with advanced computer vision techniques to enable coarse- and fine-grained analysis of physical phenomena (section 4).

Third, we evaluate state-of-the-art video generative models on **Morpheus** generating over 9000 videos, including CogVideoX [16], PyramidalFlow [17], LTX-Video [18] and COSMOS [5], and show that while these models excel in visual aesthetics, they fall short in modeling real-world physical dynamics (section 5).

Finally, we highlight key limitations and provide actionable insights for improving the physical reasoning capabilities of video generation models.

2 Related work

Evaluation of VGMs. Benchmarking video generation models have evolved to include comprehensive evaluation frameworks that assess multiple dimensions of video quality, temporal coherence, and alignment with prompts. Approaches like EvalCrafter [19], VBench [20], VBench++ [21], AIGCBench [22], and TC-Bench [23] emphasize diverse metrics to evaluate visual fidelity, motion smoothness, spatial consistency, and temporal dynamics. For example, EvalCrafter [19] uses metrics like Motion-Aware Consistency (MAC) and Scene Change Consistency (SCC) to assess the smoothness and natural progression of motion, while VBench introduces metrics for spatial relationships and subject identity consistency to evaluate logical scene composition. Despite the breadth of these benchmarks, they primarily concentrate on perceptual and semantic aspects of video generation, whereas **Morpheus** focuses on physical plausibility of the generated videos.

Physical reasoning and plausibility in VGMs. Recent advances in evaluating physical plausibility in video gen-

¹Cf. iconic “*spherical cows*” metaphor for physical assumptions

eration have employed both human assessments [1] and automated approaches leveraging vision-language models (VLMs) [1, 3] and object tracking metrics [2, 6, 5]. Notable frameworks include VideoCon-Physics [1], PhyGenBench [3] and PhysBench [24], which utilize VLMs to assess adherence to physical law prompts; VAMP [2], which quantifies motion characteristics through acceleration and velocity variance; and Physics-IQ [6] and COSMOS [5], which compare object masks between generated and real-world videos. Kang et al. [4] used the PHYRE simulator [25] to fine-tune VGM on synthetic 2D data, facilitating out-of-distribution and combinatorial generalization evaluation.

Despite addressing diverse physical phenomena, these benchmarks have significant limitations. VLM and human evaluations often identify physical deviations categorically, like noting gravity violations without quantifying them. Moreover, VLM can hallucinate [26] and miss subtle physical inconsistencies. On the other side, object tracking metrics are often based on simulated data [5, 25] and assume that modeled processes should be deterministic and predictable [4, 6]. These limitations highlight the critical need for more robust, interpretable benchmarks that can quantitatively evaluate physical realism by precisely measuring how well-generated videos preserve physical invariants and adhere to specific physical laws.

Learn physical invariants and equations from data. There is progress for learning conservation laws from trajectories [27], and equation discovery in hybrid dynamic systems [28]. Mechanistic Neural Networks (MechNN) [29] are able to learn governing Ordinary Differential Equations (ODEs) from data, while Mechanistic PDE Networks [30] can learn Partial Differential Equations (PDEs). On the other hand, to compare the theoretical prediction with input data, PINNs [14, 15], who integrate physical equations in the loss function, can help identify possible physical factors causing errors (such as unmodeled friction, air drag, etc.) because it is able to learn corrections to make the predictions closer to the actual observed values.

3 Morpheus Benchmark

To rigorously examine the discrepancies in adherence to physical laws within generated videos, we propose the **Morpheus** benchmark.

3.1 Methodology for creating the dataset

We created a dataset of real-world recordings of specific physical phenomena, focusing on fundamental aspects of Newtonian mechanics. Recordings were conducted under controlled laboratory conditions, allowing us to systematically vary initial parameters and capture repeatable scenarios. By operating in this rigorously controlled setting, we can isolate and test adherence to specific physical laws – such as the periodic dynamics of a harmonic

pendulum – rather than merely assessing overall visual plausibility. This sets our dataset apart from previous works that often focus on uncontrolled, general-purpose video data [6, 4], allowing for a more precise and targeted evaluation of physical consistency.

Physical experiments. We recorded a set of six core experiments, each highlighting specific physical principles:

1. Falling ball: A ball dropped from rest until it makes impact with the surface, used to test uniform gravitational acceleration and energy conservation.
2. Bouncing ball: A ball observed from the moment it first impacts the surface until it rebounds and impacts again, testing gravitational acceleration and energy conservation in a more challenging setting.
3. Projectile motion: A ball launched at various initial velocities and angles, testing the preservation of momentum and energy, as well as the uniformity of gravity.
4. Holonomic pendulum: A ball affixed to a rigid rod, with periodic motion and energy conservation.
5. Non-holonomic pendulum: A ball suspended by a string, showcasing approximate energy conservation and approximate harmonic motion.
6. Double pendulum: A more complex system with a pendulum attached to another pendulum, illustrating chaotic behavior and conservation laws in nonlinear dynamics.

Physical initial conditions. For each experiment, we varied specific initial conditions: the initial speed for the falling ball, the angle and initial speed for the projectile motion, and the angle for the pendulums. This diverse collection ensures robust coverage of dynamic behaviors, enabling thorough evaluation of generated videos against real-world physical phenomena. To maintain consistency in these initial parameters, we employed an actuator – namely, a robotic controller – ensuring accurate and repeatable setups. We recorded 5–7 videos per initial condition setting, resulting in approximately 10–20 videos per experiment. Complete dataset statistics and the photos of the experiments can be found in App. A.

We use the recorded dataset images in two ways mainly in our experiments. First, the initial frames of the real-world videos serve as prompts to set the initial conditions for the conditional video generation models. This ensures that the generated sequences begin from the same starting point as the real-world experiments.

Second, we use real-world videos as a “gold standard” to validate that our evaluation metrics work as intended. By analyzing the metrics on these ground-truth recordings, we demonstrate the reliability of our approach and establish an upper bound on performance, representing the precision with which we can measure adherence to physical laws. In essence, the metrics computed on real-world videos pro-

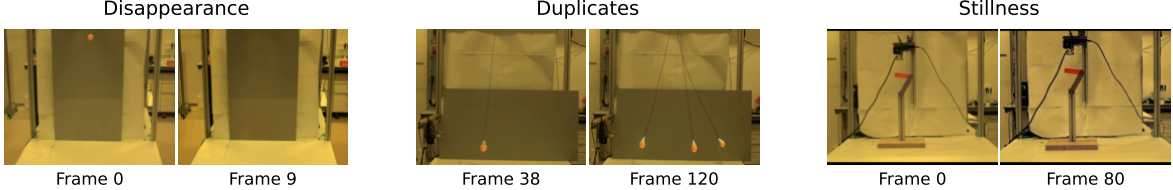


Figure 2: Different types of discarded generated videos: (left) A video showing the disappearance of the orange ball during fall; (middle) A video illustrating generation of multiple non-holonomic pendulums; (right) A video in which the double pendulum does not move.

vide a baseline for how closely any generative model can align with physical principles.

To structurally analyze the videos, we extract the trajectories of the objects by applying promptable visual segmentation. These trajectories comprise 2D coordinates of the recognized objects through time and are used for further analysis with our physical metrics. We describe the trajectory extraction in Sec. 3.3.

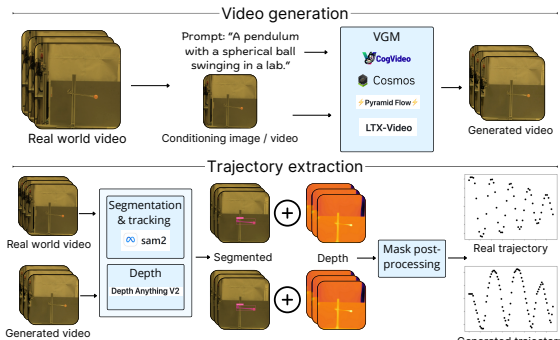


Figure 3: The video generation (upper) and the trajectory extraction pipeline (lower). We use the first frame (or multiple frames in case of video conditioning) of the real-world recording of an experiment, as well as the textual description, as a prompt for a Video Generation Model (VGM). Next, we extract object trajectories for both real-world and generated videos using trajectory extraction pipeline, consisting of Segmentation and Tracking (SAM2), and relative depth estimation (DepthAnything V2) and postprocessing.

3.2 Prompting methods

The physical dynamics of a scene are fundamentally determined by its initial conditions, which include the positions, velocities, and geometric constraints (e.g. shapes, rigid body connections) of all objects at the outset. In the context of generative models, these initial conditions are set through prompting. There are three main approaches to prompting: *a)* textual prompts, *b)* single-image prompts, and *c)* video (or multi-frame) prompts. Each provides a different level of control over the generation process.

Textual prompts offer minimal control. They can suggest the general behavior or nature of a scene - such as a ball

rolling or falling - but lack the precision to define exact starting positions, velocities, or trajectories. *Single-image prompts* improve upon this by allowing the initial positions of objects to be visually specified. However, they still fall short in terms of velocity and motion details. Only *video prompts*, which incorporate sequences of frames, grant the ability to set both initial positions and velocities of all currently visible objects. This introduces a gradation in the level of control: from the broad suggestions of textual prompts to the detailed specifications of video prompts.

With this gradation in mind, we investigate how different levels of control affect the physical realism of the generated samples. We explore both textual prompt enhancement and various multi-frame prompting for models capable of leveraging these features (e.g. [5, 16]), allowing us to examine the relationship between input precision and output physical fidelity. Following the approach of [16], simple scene descriptions can be enhanced with the advanced capabilities of a VLM [31] in creating rich and descriptive prompts along when provided with a certain instruction template in either a zero-shot or few-shot fashion. As not all VGMs provide a prompt upsampler along the model, we rely on the ChatGLM family of models [31], while for COSMOS [5] we use their own devised [32, 33] upsamplers. In our evaluation, we still try to create a highly descriptive prompt with an emphasis on capturing the physical motion, and the upsampler allows us to bring the distribution of the textual prompt during inference closer to the one used during training.

3.3 Trajectory extraction

While generated videos could be directly evaluated in terms of 3D consistency [19] or other pixel-level generation properties [5], such evaluations are limited to visual and geometric realism of the generated videos. Instead, we are interested in how well these videos conform to physical laws. This means that we need to extract the relevant physical state variables, such as positions of objects, velocities, accelerations, masses, and so on. Thus, it is essential to transform the generated videos into perfect state variables of the depicted objects and their trajectories, which can then be further analyzed.

A supervised object-tracking model would work well for specific video domains. However, for unseen generated

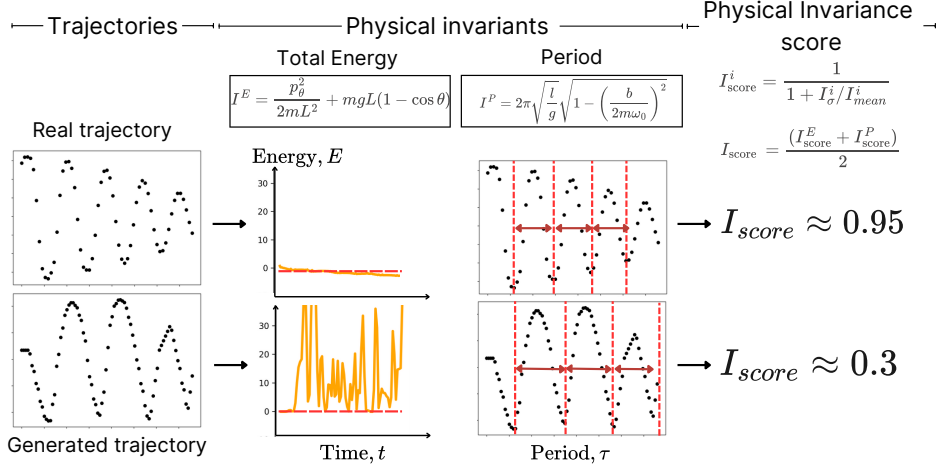


Figure 4: Evaluation of trajectories extracted from real and VGMs videos using Physical Invariance score derived from physical invariants.

videos, we need more general methods for reliable processing. Thus, we propose leveraging a vision foundation model for zero-shot object segmentation and tracking. In particular, we use Segment Anything 2 (SAM2) [34], a promptable segmentation and tracking model for images and videos that provides 2D masks. We label the first frames of the videos in our dataset using positive and negative clicks as spatial prompts and verify the segmentation before tracking the object throughout the video. Finally, we extract center-of-mass 2D coordinates by averaging object mask centers. In addition, to check if objects have consistent depth (necessary for using only 2D coordinates for our physical scores, see App. C.2), we estimate relative object depth using Depth Anything V2 [35] to predict depth values for the corresponding masks from SAM2 (see Fig. 3 for illustration).

For velocity, acceleration and angular velocity, we employ the *central difference method* [36]. To further reduce the noise, generated by the imperfections in the tracking pipeline, we follow with a series of smoothing operations, such as learning a linear regression with a sliding window and applying the Savitzky-Golay smoothing. The details can be found in the App. B.

Since the generated videos may contain artifacts that prohibit further analysis, e.g. objects’ permanence, jittering, or absence of movement, we discard such samples and keep track of the *discard rate* for each model.

4 Physics-informed evaluation metrics

To assess the alignment of the generated video trajectories with physical laws, we propose a hierarchical evaluation framework for analyzing physical experiments in both real-world and generated videos.

Discard rate As a first metric, we compute the *discard rate*, which reflects the proportion of model-generated sam-

ples that must be discarded to ensure reliable trajectory extraction needed for Physical Invariances and Dynamical scores. The discard filtering is automatic and consists of three criteria: First, we discard generated videos where objects lack sufficient permanence throughout the video. Second, we discard generated videos which do not have a consistent number of objects. Finally, we discard generated videos if there is little motion detected, as such videos are not suitable for physical analysis. The overall discard rate represents the proportion of generated videos that fail at least one of these criteria. In addition, we verify that none of the real-world extracted trajectories are discarded, showing that our discard criteria are effective in distinguishing physical from non-physical videos. We provide further details on our filtering methodology in App. C.1.

Beyond pixel-by-pixel evaluation For the videos that pass the filtering, we employ two metrics: *the Dynamical score*, which measures the overall adherence to the equation of motion that governs the system, and *the Physical Invariance score*, which quantifies the invariance of conserved physical quantities, such as energy or angular momentum (Table A2).

As discussed above, pixel-by-pixel evaluation is inherently problematic when perfect control over the initial conditions is not achievable. Even with ideal control, the chaotic nature of certain physical phenomena can cause minor differences in initial conditions to produce vastly divergent outcomes. Consequently, straightforward time-based trajectory matching becomes an unreliable measure of performance. For our benchmark, we instead rely on metrics that do not depend on direct time-aligned comparisons. These metrics are designed to evaluate physical consistency and adherence to fundamental laws independently of precise time synchronization, providing a more robust and generalizable standard of evaluation. In our approach, the obtained real-world trajectories act as reference points

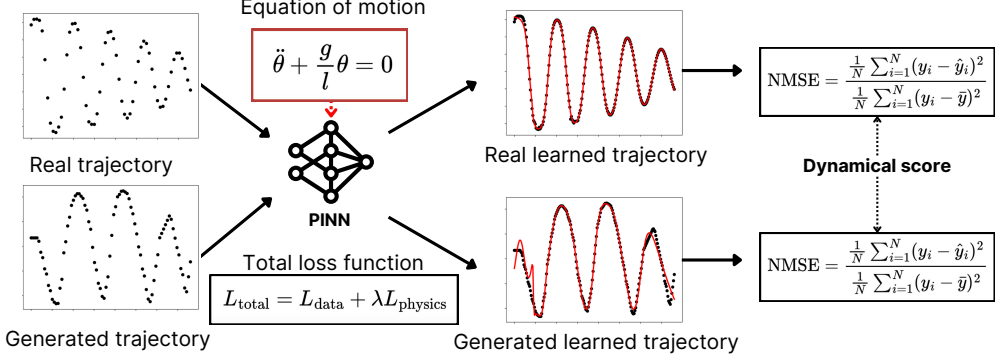


Figure 5: Evaluation of trajectories extracted from real and VGMs videos using Dynamical score. For each of the trajectory, real-world or generated videos, we fit a PINN with the corresponding equation of motion for the particular physical law as an extra loss term.

to establish the upper bounds of performance and validate our methods.

4.1 Dynamical score

To calculate the Dynamical score, we use physics-informed neural networks (PINNs)[14], which directly incorporate physical laws as a prior. This setting allows us to learn the physical trajectory that fits the data the most, independent of the initial conditions. Fig. 5 illustrates our approach. A PINN is a neural network that receives a timestep i of the trajectory as input and outputs the trajectory coordinates \hat{T}_i , velocity $\dot{\hat{T}}_i$, and acceleration $\ddot{\hat{T}}_i$. The model is typically trained with a loss function, comprising two components L_{data} and L_{physics} : $L_{\text{total}} = L_{\text{data}} + \lambda L_{\text{physics}}$, where the L_{data} is responsible for fitting the model to the datapoints, $L_{\text{data}} = \frac{1}{N} \sum_{i=1}^N \|\hat{T}_i - T_i\|^2$, and L_{physics} enforces following the physical law. For each experiment, we explicitly implement the equation of motion in the form of an ordinary differential equation as PINN loss functions. E.g., for the falling ball, the equations of motion are: $\dot{x} = 0$; $\ddot{y} + g = 0$, where y is the vertical position, \ddot{y} is the acceleration and g is the gravitational constant. The L_{physics} is calculated as: $L_{\text{physics}} = \frac{1}{M} \sum_{j=1}^M \|\hat{y}_j + g\|^2 + \|\dot{\hat{x}}\|^2$, where \hat{y}_j is the predicted acceleration derived from the PINN at the j -th time step.

Computing the Dynamical score. In our context, we use PINNs to assess the physical plausibility of trajectories from generated videos by computing the normalized mean square error (NMSE) of the model-learned trajectory derived from real and generated videos. To normalize it into the range of $(0, 1)$, we inverse the error with 1 indicating a maximal Dynamical score and 0 indicating worse than constant function fit of the corresponding PINN. Dynamical score shows the difference between theoretical prediction from the ODEs and trajectory data. A higher Dynamical score implies higher physical plausibility. For more details, please see App. C.3.

4.2 Physical Invariance score

To calculate a more fine-grained Physical Invariance score, we accompany each of our experiments with a list of physical invariances, i.e. values that we can derive from trajectories that stay constant in time. For the physical model to work, we make a series of reasonable assumptions about the setting and test them on the real-world trajectories. As invariances vary for different experiments, we present here one case study for the falling ball experiments, while describing all the other settings in App. C.4. We list in Table A2 all theoretically conserved values per experimental scenario.

Case study: Falling ball. In the falling ball experiments, we have the following physical invariants.

⇒ *Total energy.* Assuming negligible air resistance, the total energy—the sum of the kinetic and potential energy—of the ball is conserved. The kinetic energy of the ball is: $T = \frac{1}{2}m(v_x^2 + v_y^2)$, where $v = (v_x, v_y)$ is the speed of the ball and m is its mass. Also, the potential energy is $V = mgy$ where g is the gravitational acceleration constant and y is the vertical coordinate. So, as the total energy is the sum of kinetic and potential, we get: $E = T + V = \frac{1}{2}m(v_x^2 + v_y^2) + mgy$.

⇒ *Energy-to-mass ratio.* Assuming that the mass of the ball is constant, we derive the following invariant: $\frac{E}{m} = \frac{1}{2}(v_x^2 + v_y^2) + gy = \text{const}$, which we can estimate with the data from our trajectory.

⇒ *Acceleration.* As no external forces are acting on the ball except for gravity, which is uniform in space and time and is directed downwards, the acceleration of the ball is also constant: $a_y = g = \text{const}$.

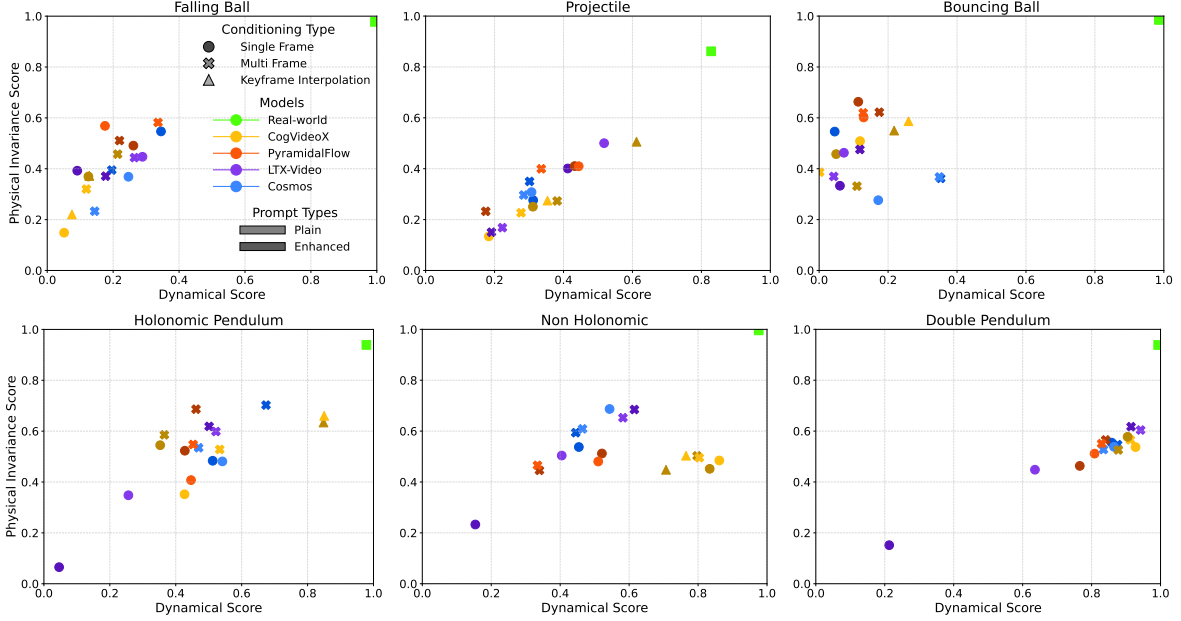


Figure 6: Physical Invariance vs. Dynamical scores for all the experiments. Different colors correspond to different models, whereas the hue of the color differentiates between base and enhanced prompts. Scores from trajectories extracted from real-world videos are consistently close to maximum scores, while deviations are explained by trajectory estimation errors and using only 2D trajectories.

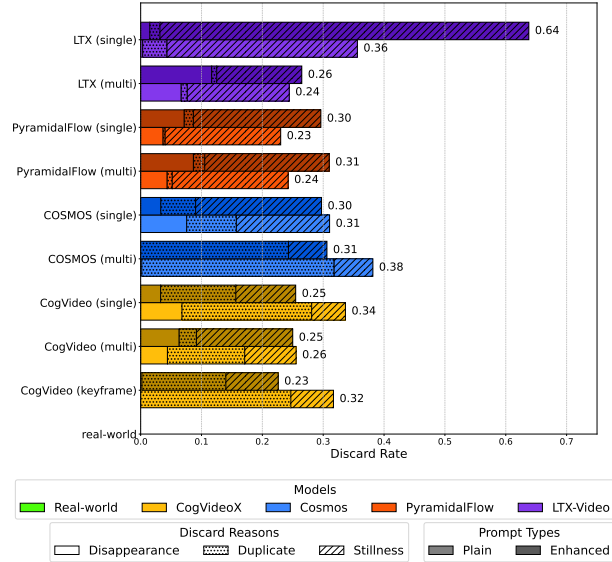


Figure 7: Average discard rates across all physical experiments.

⇒ *Horizontal momentum-to-mass ratio.* As with acceleration, the horizontal momentum, $p_x = mV_x$, is also preserved given no external forces. This implies that the horizontal velocity is conserved: $v_x = \text{const}$

Computing the Physical Invariance score. To convert the invariant into an actual score, like the Energy score, we

calculate the standard deviation of the invariant time series and normalize it into the range of $(0, 1)$, with 1 indicating a perfect Physical Invariance score.

As invariants must be by nature constant, a high standard deviation of these invariants (and thus a lower physical invariance score), indicates poor modeling of the respective physical invariants. In addition, for discarded trajectories we assign minimal Physical Invariance score equal to 0. A detailed score calculation procedure is described in the App. C.5. For the derivations of each invariant we used, please refer to the App. C.4.

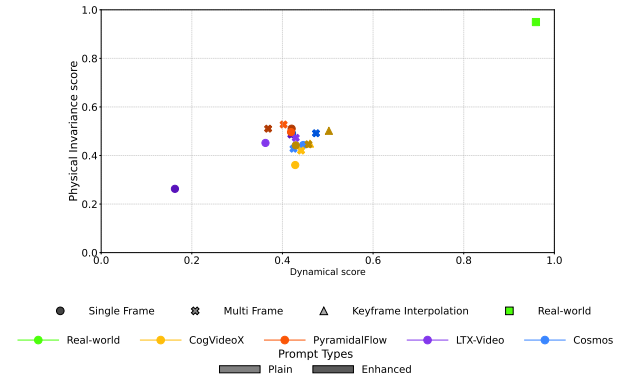


Figure 8: Average Physical Invariance vs. Dynamical scores over the experiments. Different colors correspond to different models, whereas the hue of the color differentiates between base and enhanced prompts.

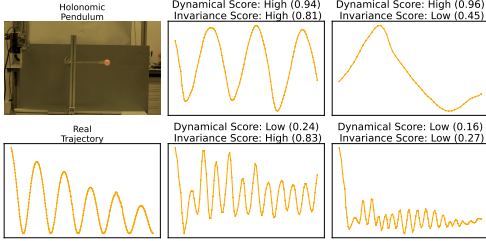


Figure 9: Real pendulum trajectory alongside four cases of generated videos, demonstrating how different combinations of dynamical and physical invariance scores appear in practice.

5 Analysis

In this section, we analyze the results of the experiments. In tables A5 to A9, as well as Fig. 6 and Fig. 8, we note *plain* for simple text prompts, and *enhanced* for upgraded textual description (see Sec.3.2). We consider the multi-frame prompting scenario separately.

Real-world videos consistently deliver optimal results across all experiments, as demonstrated by their minimal discard rates, high Dynamical scores (0.98–0.99), and consistently high Physical Invariance scores (above 0.93). These metrics confirm the reliability of real-world videos as benchmarks for physically accurate and realistic motion, and validate the correctness of our experimental setups, providing the upper boundary for the performance of the video generation models.

Enhanced prompts typically improve performance metrics compared to plain prompts, although this trend varies depending on the specific model. Enhanced prompting leads to higher physical invariance and dynamical scores and lower discard rates in many cases (e.g., COSMOS and CogVideoX), yet occasionally decreases performance in models such as LTX and PyramidalFlow, indicating that prompt enhancement effectiveness is context-dependent.

Multi-frame prompting generally outperforms single-frame prompting, achieving lower discard rates and higher dynamical and physical invariance scores, thereby demonstrating the advantage of increased temporal context. The prompting with first and last frames, used exclusively by CogVideoX as an interpolation regime, performs notably well in specific experiments (e.g., holonomic pendulum), suggesting a promising direction for improving temporal coherence and physical realism, though limiting the ability to generate from scratch.

Among the evaluated models, CogVideoX typically demonstrates superior performance, especially in multi-frame configurations with enhanced prompts. LTX, while occasionally excelling in specific scenarios (such as single-frame enhanced prompts for the falling ball), exhibits inconsistent performance, with high variability and notably high discard rates in certain tasks. COSMOS and PyramidalFlow show intermediate performance, with COSMOS

performing strongly in multi-frame scenarios and PyramidalFlow achieving moderate results.

The variability of discard rates across setups reflects the reliability of different models in generating physically plausible videos. Discard rates vary significantly, with extremes ranging from as low as 0.0% (COSMOS single-frame, plain prompt, double pendulum) to as high as 92% (LTX single-frame, enhanced prompt, holonomic pendulum). The analysis of the major reasons (see Fig.7) behind high discard rates reveals the absence of motion (i.e. *stillness*) and the presence of duplicate objects, as well as, to a lesser extent, the disappearance of the object from the video. These persistent shortcomings in the models’ abilities to produce consistent and realistic videos are well-known [21].

Analyzing fine-grained conservation metrics across experiments reveals several interesting trends. In the falling and bouncing ball scenarios, relatively high horizontal momentum conservation scores can primarily be attributed to the absence of significant horizontal motion rather than accurate modeling of dynamics. In contrast, for the projectile task, where horizontal motion is inherently present, horizontal momentum conservation scores align closely with the generally lower scores observed for energy and acceleration conservation, reflecting the genuine complexity of modeling horizontal dynamics. Additionally, multi-frame prompting substantially enhances distance conservation metrics, likely because maintaining spatial relationships between objects across frames is fundamentally simpler than modeling intricate dynamical properties. Moderate improvements in energy and period conservation further support the advantage of multi-frame temporal context. In pendulum scenarios, some periodic behavior emerges in generated videos (see Fig. 9 and Fig. A10), suggesting that models partly capture periodicity; however, adherence to true dynamical behavior remains limited, as demonstrated by, for example, the low-energy conservation scores.

Overall, all generated models exhibit substantial limitations compared to real-world performance (see Fig. 8), underscoring the significant gaps remaining in simulating realistic and physically accurate dynamics. We present additional per experiment and prompt analysis in the App. F.

6 Limitations

As the first to analyze detailed physics invariances in generative models, we note individual scores can be misleading alone. For example, a levitating object might preserve energy (appearing correct) while violating gravity. Thus, Physical Invariance scores must be combined with Dynamical ones to get a complete and detailed picture of generative model performance.

7 Conclusion

Our study highlights a fundamental limitation in current video generation models: despite their impressive realism, they fail to consistently adhere to physical laws. To address this gap, we introduced Morpheus, a benchmark designed to assess the physical reasoning capabilities of these models. Through a curated dataset of real-world physics experiments and physics-informed evaluation met-

rics, we demonstrate that even with advanced prompting techniques, existing models struggle to capture fundamental physical principles. In general, all models perform poorly, with significant violations of physical principles, though multi-frame prompting provides some improvement. This underscores the need for future research in integrating physical constraints into generative models. We open-source our dataset, baselines, and code to foster further advancements in physics-aware video generation at physics-from-video.github.io/morpheus-bench.

Acknowledgments

AZ is funded by the European Union (ERC, EVA, 950086). We thank Prof. Maziyar Jalaal for providing the equipment for physical experiments.

Contributions

CZ came up with the idea of measuring the physical reasoning ability of video generation models. EG, DC, AZ and CZ set up the initial meeting to structure the project into three parts: experiments recording, trajectory tracking and extracting, and scores calculation. DC and AT collected all the real-world videos with the help of DP. AT, TN and DP set up video generation code for all models with the help from AZ. AZ set up object segmentation and tracking and integrated all parts of the benchmark into automated pipeline with the help from TN and AT. AV completed the Dynamical scores evaluation, while CZ designed the Physical Invariant Scores. The paper was written by CZ, DC, AZ and EG with DC and DP contributing to Fig. 1, 3, 4, 5, AV created Fig. 9 and TN contributed to Fig. 2. AZ created Table 1 and made all the experimental results aggregation and visualization in Fig. 6, 7, 8 with the help from MB. The website development was coordinated by AZ with contributions from CZ (leaderboard), DC (videos), MB (overall structure and plots).

References

- [1] Hritik Bansal, Zongyu Lin, Tianyi Xie, Zeshun Zong, Michal Yarom, Yonatan Bitton, Chenfanfu Jiang, Yizhou Sun, Kai-Wei Chang, and Aditya Grover. Videophy: Evaluating physical commonsense for video generation. *arXiv preprint arXiv:2406.03520*, 2024.
- [2] Zihan Wang, Songlin Li, Lingyan Hao, Bowen Song, and Xinyu Hu. What you see is what matters: A novel visual and physics-based metric for evaluating video generation quality. *arXiv preprint arXiv:2411.13609*, 2024.
- [3] Fanqing Meng, Jiaqi Liao, Xinyu Tan, Wenqi Shao, Quanfeng Lu, Kaipeng Zhang, Yu Cheng, Dianqi Li, Yu Qiao, and Ping Luo. Towards world simulator: Crafting physical commonsense-based benchmark for video generation. *arXiv preprint arXiv:2410.05363*, 2024.
- [4] Bingyi Kang, Yang Yue, Rui Lu, Zhijie Lin, Yang Zhao, Kaixin Wang, Gao Huang, and Jiashi Feng. How far is video generation from world model: A physical law perspective. *arXiv preprint arXiv:2411.02385*, 2024.
- [5] Niket Agarwal, Arslan Ali, Maciej Bala, Yogesh Balaji, Erik Barker, Tiffany Cai, Prithvijit Chattopadhyay, Yongxin Chen, Yin Cui, Yifan Ding, et al. Cosmos world foundation model platform for physical ai, 2025.
- [6] Saman Motamed, Laura Culp, Kevin Swersky, Priyank Jaini, and Robert Geirhos. Do generative video models learn physical principles from watching videos? *arXiv preprint arXiv:2501.09038*, 2025.
- [7] Tim Brooks, Bill Peebles, Connor Holmes, Will DePue, Yufei Guo, Li Jing, David Schnurr, Joe Taylor, Troy Luhman, Eric Luhman, Clarence Ng, Ricky Wang, and Aditya Ramesh. Video generation models as world simulators. 2024.
- [8] Veo-Team, :, Agrim Gupta, Ali Razavi, Andeep Toor, Ankush Gupta, Dumitru Erhan, Eleni Shaw, Eric Lau, Frank Belletti, Gabe Barth-Maron, Gregory Shaw, Hakan Erdogan, Hakim Sidahmed, Henna Nandwani, Hernan Moraldo, Hyunjik Kim, Irina Blok, Jeff Donahue, José Lezama, Kory Mathewson, Kurtis David, Matthieu Kim Lorrain, Marc van Zee, Medhini Narasimhan, Miaosen Wang, Mohammad Babaizadeh, Nelly Papalampidi, Nick Pezzotti, Nilpa Jha, Parker Barnes, Pieter-Jan Kindermans, Rachel Hornung, Ruben Villegas, Ryan Poplin, Salah Zaiem, Sander Dieleman, Sayna Ebrahimi, Scott Wisdom, Serena Zhang, Shlomi Fruchter, Signe Nørly, Weizhe Hua, Xinchen Yan, Yuqing Du, and Yutian Chen. Veo 2. 2024.
- [9] Aditya Ramesh, Mikhail Pavlov, Gabriel Goh, Scott Gray, Chelsea Voss, Alec Radford, Mark Chen, and Ilya Sutskever. Zero-shot text-to-image generation. In *International conference on machine learning*, pages 8821–8831. Pmlr, 2021.
- [10] Chitwan Saharia, William Chan, Saurabh Saxena, Lala Li, Jay Whang, Emily L Denton, Kamyar Ghasemipour, Raphael Gontijo Lopes, Burcu Karagol Ayan, Tim Salimans, et al. Photorealistic text-to-image diffusion models with deep language understanding. *Advances in neural information processing systems*, 35:36479–36494, 2022.
- [11] Dustin Podell, Zion English, Kyle Lacey, Andreas Blattmann, Tim Dockhorn, Jonas Müller, Joe Penna, and Robin Rombach. Sdxl: Improving latent diffusion models for high-resolution image synthesis. *arXiv preprint arXiv:2307.01952*, 2023.
- [12] Lili Yu, Bowen Shi, Ramakanth Pasunuru, Benjamin Muller, Olga Golovneva, Tianlu Wang, Arun Babu, Binh Tang, Brian Karrer, Shelly Sheynin, et al. Scaling autoregressive multi-modal models: Pretraining and instruction tuning. *arXiv preprint arXiv:2309.02591*, 2(3), 2023.
- [13] Joseph Cho, Fachrina Dewi Puspitasari, Sheng Zheng, Jingyao Zheng, Lik-Hang Lee, Tae-Ho Kim, Choong Seon Hong, and Chaoning Zhang. Sora as an agi world model? a complete survey on text-to-video generation. *arXiv preprint arXiv:2403.05131*, 2024.
- [14] Salvatore Cuomo, Vincenzo Schiano Di Cola, Fabio Giampaolo, Gianluigi Rozza, Maziar Raissi, and Francesco Piccialli. Scientific machine learning through physics-informed neural networks: Where we are and what's next. *Journal of Scientific Computing*, 92(3):88, 2022.

- [15] GaoYuan He, YongXiang Zhao, and ChuLiang Yan. Mflp-pinn: A physics-informed neural network for multiaxial fatigue life prediction. *European Journal of Mechanics-A/Solids*, 98:104889, 2023.
- [16] Zhuoyi Yang, Jiayan Teng, Wendi Zheng, Ming Ding, Shiyu Huang, Jiazheng Xu, Yuanming Yang, Wenyi Hong, Xiaohan Zhang, Guanyu Feng, et al. Cogvideox: Text-to-video diffusion models with an expert transformer. *CoRR*, 2024.
- [17] Yang Jin, Zhicheng Sun, Ningyuan Li, Kun Xu, Hao Jiang, Nan Zhuang, Quzhe Huang, Yang Song, Yadong Mu, and Zhouchen Lin. Pyramidal flow matching for efficient video generative modeling. *arXiv preprint arXiv:2410.05954*, 2024.
- [18] Yoav HaCohen, Nisan Chiprut, Benny Brazowski, Daniel Shalem, Dudu Moshe, Eitan Richardson, Eran Levin, Guy Shiran, Nir Zabari, Ori Gordon, et al. Ltx-video: Realtime video latent diffusion. *arXiv preprint arXiv:2501.00103*, 2024.
- [19] Yaofang Liu, Xiaodong Cun, Xuebo Liu, Xintao Wang, Yong Zhang, Haoxin Chen, Yang Liu, Tieyong Zeng, Raymond Chan, and Ying Shan. Evalcrafter: Benchmarking and evaluating large video generation models. In *Proceedings of the IEEE/CVF Conference on Computer Vision and Pattern Recognition*, pages 22139–22149, 2024.
- [20] Ziqi Huang, Yinan He, Jiashuo Yu, Fan Zhang, Chenyang Si, Yuming Jiang, Yuanhan Zhang, Tianxing Wu, Qingyang Jin, Nattapol Champaisit, et al. Vbench: Comprehensive benchmark suite for video generative models. In *Proceedings of the IEEE/CVF Conference on Computer Vision and Pattern Recognition*, pages 21807–21818, 2024.
- [21] Ziqi Huang, Fan Zhang, Xiaojie Xu, Yinan He, Jiashuo Yu, Ziyue Dong, Qianli Ma, Nattapol Champaisit, Chenyang Si, Yuming Jiang, et al. Vbench++: Comprehensive and versatile benchmark suite for video generative models. *arXiv preprint arXiv:2411.13503*, 2024.
- [22] Fanda Fan, Chunjie Luo, Wanling Gao, and Jianfeng Zhan. Aigcbench: Comprehensive evaluation of image-to-video content generated by ai. *BenchCouncil Transactions on Benchmarks, Standards and Evaluations*, page 100152, 2024.
- [23] Weixi Feng, Jiachen Li, Michael Saxon, Tsu-jui Fu, Wenhui Chen, and William Yang Wang. Tc-bench: Benchmarking temporal compositionality in text-to-video and image-to-video generation. *arXiv preprint arXiv:2406.08656*, 2024.
- [24] Wei Chow, Jiageng Mao, Boyi Li, Daniel Seita, Vitor Guizilini, and Yue Wang. Physbench: Benchmarking and enhancing vision-language models for physical world understanding. *arXiv preprint arXiv:2501.16411*, 2025.
- [25] Anton Bakhtin, Laurens van der Maaten, Justin Johnson, Laura Gustafson, and Ross Girshick. Phyre: A new benchmark for physical reasoning. *Advances in Neural Information Processing Systems*, 32, 2019.
- [26] Yifan Li, Yifan Du, Kun Zhou, Jinpeng Wang, Wayne Xin Zhao, and Ji-Rong Wen. Evaluating object hallucination in large vision-language models. *arXiv preprint arXiv:2305.10355*, 2023.
- [27] Ziming Liu and Max Tegmark. Machine learning conservation laws from trajectories. *Physical Review Letters*, 126(18):180604, 2021.
- [28] Yongtuo Liu, Sara Magliacane, Miltiadis Kofinas, and Efstratios Gavves. Amortized equation discovery in hybrid dynamical systems. *arXiv preprint arXiv:2406.03818*, 2024.
- [29] Adeel Pervez, Francesco Locatello, and Efstratios Gavves. Mechanistic neural networks for scientific machine learning. *arXiv preprint arXiv:2402.13077*, 2024.
- [30] Adeel Pervez, Efstratios Gavves, and Francesco Locatello. Mechanistic pde networks for discovery of governing equations. *arXiv preprint arXiv:2502.18377*, 2025.
- [31] Aohan Zeng, Bin Xu, Bowen Wang, Chenhui Zhang, Da Yin, Dan Zhang, Diego Rojas, Guanyu Feng, Hanlin Zhao, Zhihan Liu, Zhiyuan Liu, Jialiang Tang, Qiang Liu, and Jie Tang. Chatglm: A family of large language models from glm-130b to glm-4 all tools. *arXiv preprint arXiv:2406.12793*, 2024.
- [32] NVIDIA. Mistral and nvidia. mistral-nemo-12b-instruct: A 12b parameter large language model., <https://huggingface.co/nvidia/Mistral-NeMo-12B-Instruct>, 2024.
- [33] Pravesh Agrawal, Szymon Antoniak, Emma Bou Hanna, Baptiste Bout, Devendra Chaplot, Jessica Chudnovsky, Diogo Costa, Baudouin De Monicault, Saurabh Garg, Theophile Gervet, et al. Pixtral 12b. *arXiv preprint arXiv:2410.07073*, 2024.
- [34] Nikhila Ravi, Valentin Gabeur, Yuan-Ting Hu, Ronghang Hu, Chaitanya Ryali, Tengyu Ma, Haitham Khedr, Roman Rädle, Chloe Rolland, Laura Gustafson, et al. Sam 2: Segment anything in images and videos. *arXiv preprint arXiv:2408.00714*, 2024.
- [35] Lihe Yang, Bingyi Kang, Zilong Huang, Zhen Zhao, Xiaogang Xu, Jiashi Feng, and Hengshuang Zhao. Depth anything v2. *arXiv:2406.09414*, 2024.
- [36] R Charles Swanson and Eli Turkel. On central-difference and upwind schemes. *Journal of computational physics*, 101(2):292–306, 1992.
- [37] Jianwen Luo, Kui Ying, and Jing Bai. Savitzky–golay smoothing and differentiation filter for even number data. *Signal Processing*, 85(7):1429–1434, 2005.
- [38] Ho Kei Cheng, Seoung Wug Oh, Brian Price, Alexander Schwing, and Joon-Young Lee. Tracking anything with decoupled video segmentation. In *ICCV*, 2023.
- [39] Tianhe Ren, Shilong Liu, Ailing Zeng, Jing Lin, Kunchang Li, He Cao, Jiayu Chen, Xinyu Huang, Yukang Chen, Feng Yan, et al. Grounded sam: Assembling open-world models for diverse visual tasks. *arXiv preprint arXiv:2401.14159*, 2024.

- [40] Shilong Liu, Zhaoyang Zeng, Tianhe Ren, Feng Li, Hao Zhang, Jie Yang, Qing Jiang, Chunyuan Li, Jianwei Yang, Hang Su, et al. Grounding dino: Marrying dino with grounded pre-training for open-set object detection. In *European Conference on Computer Vision*, pages 38–55. Springer, 2025.
- [41] Diederik P Kingma. Auto-encoding variational bayes. *arXiv preprint arXiv:1312.6114*, 2013.
- [42] Bin Lin, Yunyang Ge, Xinhua Cheng, Zongjian Li, Bin Zhu, Shaodong Wang, Xianyi He, Yang Ye, Shenghai Yuan, Liuhan Chen, et al. Open-sora plan: Open-source large video generation model. *arXiv preprint arXiv:2412.00131*, 2024.
- [43] Colin Raffel, Noam Shazeer, Adam Roberts, Katherine Lee, Sharan Narang, Michael Matena, Yanqi Zhou, Wei Li, and Peter J Liu. Exploring the limits of transfer learning with a unified text-to-text transformer. *Journal of machine learning research*, 21(140):1–67, 2020.
- [44] Ling Yang, Zhilong Zhang, Yang Song, Shenda Hong, Runsheng Xu, Yue Zhao, Wentao Zhang, Bin Cui, and Ming-Hsuan Yang. Diffusion models: A comprehensive survey of methods and applications. *ACM Computing Surveys*, 56(4):1–39, 2023.
- [45] Olaf Ronneberger, Philipp Fischer, and Thomas Brox. U-net: Convolutional networks for biomedical image segmentation. In *Medical image computing and computer-assisted intervention–MICCAI 2015: 18th international conference, Munich, Germany, October 5–9, 2015, proceedings, part III 18*, pages 234–241. Springer, 2015.
- [46] Daquan Zhou, Weimin Wang, Hanshu Yan, Weiwei Lv, Yizhe Zhu, and Jiashi Feng. Magicvideo: Efficient video generation with latent diffusion models. *arXiv preprint arXiv:2211.11018*, 2022.
- [47] Omer Bar-Tal, Hila Chefer, Omer Tov, Charles Herrmann, Roni Paiss, Shiran Zada, Ariel Ephrat, Junhwa Hur, Guanghui Liu, Amit Raj, et al. Lumiere: A space-time diffusion model for video generation. In *SIGGRAPH Asia 2024 Conference Papers*, pages 1–11, 2024.
- [48] Weijie Kong, Qi Tian, Zijian Zhang, Rox Min, Zuozhuo Dai, Jin Zhou, Jiangfeng Xiong, Xin Li, Bo Wu, Jianwei Zhang, Kathrina Wu, Qin Lin, Aladdin Wang, Andong Wang, Changlin Li, Duojun Huang, Fang Yang, Hao Tan, Hongmei Wang, Jacob Song, Jiawang Bai, Jianbing Wu, Jinbao Xue, Joey Wang, Junkun Yuan, Kai Wang, Mengyang Liu, Pengyu Li, Shuai Li, Weiyang Wang, Wenqing Yu, Xinchi Deng, Yang Li, Yanxin Long, Yi Chen, Yutao Cui, Yuanbo Peng, Zhentao Yu, Zhiyu He, Zhiyong Xu, Zixiang Zhou, Yangyu Tao, Qinglin Lu, Songtao Liu, Dax Zhou, Hongfa Wang, Yong Yang, Di Wang, Yuhong Liu, Jie Jiang, and Caesar Zhong. Hunyuandvideo: A systematic framework for large video generative models, 2024.
- [49] Tim Brooks, Bill Peebles, Connor Holmes, Will DePue, Yufei Guo, Li Jing, David Schnurr, Joe Taylor, Troy Luhman, Eric Luhman, et al. Video generation models as world simulators, 2024.
- [50] Wenming Weng, Ruoyu Feng, Yanhui Wang, Qi Dai, Chunyu Wang, Dacheng Yin, Zhiyuan Zhao, Kai Qiu, Jianmin Bao, Yuhui Yuan, et al. Art-v: Auto-regressive text-to-video generation with diffusion models. In *Proceedings of the IEEE/CVF Conference on Computer Vision and Pattern Recognition*, pages 7395–7405, 2024.
- [51] Haoge Deng, Ting Pan, Haiwen Diao, Zhengxiong Luo, Yufeng Cui, Huchuan Lu, Shiguang Shan, Yonggang Qi, and Xinlong Wang. Autoregressive video generation without vector quantization. *arXiv preprint arXiv:2412.14169*, 2024.
- [52] Dirk Weissenborn, Jakob Uszkoreit, and Oscar Täckström. Scaling autoregressive video models. In *ICLR*, 2020.
- [53] Jinbo Xing, Menghan Xia, Yong Zhang, Haoxin Chen, Wangbo Yu, Hanyuan Liu, Gongye Liu, Xintao Wang, Ying Shan, and Tien-Tsin Wong. Dynamicrafter: Animating open-domain images with video diffusion priors. In *European Conference on Computer Vision*, pages 399–417. Springer, 2025.
- [54] Kling AI. Kling ai. <https://klingai.com/>, 2024.

APPENDIX

A Dataset

Dataset Description: The dataset comprises recordings of five distinct real-world dynamic systems: a falling ball, a non-holonomic pendulum, a holonomic pendulum, and a projectile motion. For each system, we recorded multiple times the type of experiment trying to have homogenous videos, while after a few iterations, we varied the initial conditions or configuration parameters. Table A1 below summarizes the number of recordings and configurations for each experiment.

Experiment	Videos	Factors of Variation	Configuration/ Initial Condition Description
Falling Ball	12	1	Height from which the ball was released.
Projectile	15	3	Angle of launch, slingback extension levels, launched ball color.
Bouncing ball	12	1	Heights from which the ball was released before bouncing.
Holonomic Pendulum	22	1	Initial angle from the vertical (zero-degree resting position).
Non-Holonomic Pendulum	15	1	Initial angle from the vertical (zero-degree resting position).
Double Pendulum	10	1	Initial height of the second (top) pendulum bob.

Table A1: Summary of the Experimental Dataset from real-world recorded videos.

Falling ball For the falling ball experiment, we used a normal table tennis orange ball. A mechanic actuator ² was used to hold the ball at a certain height (initial position) and as a release mechanism to control the moment the ball was let at a free fall, before making contact with the surface below. Different height levels from the surface were used as initial positions, resulting in trajectories with different lengths (smaller or larger).

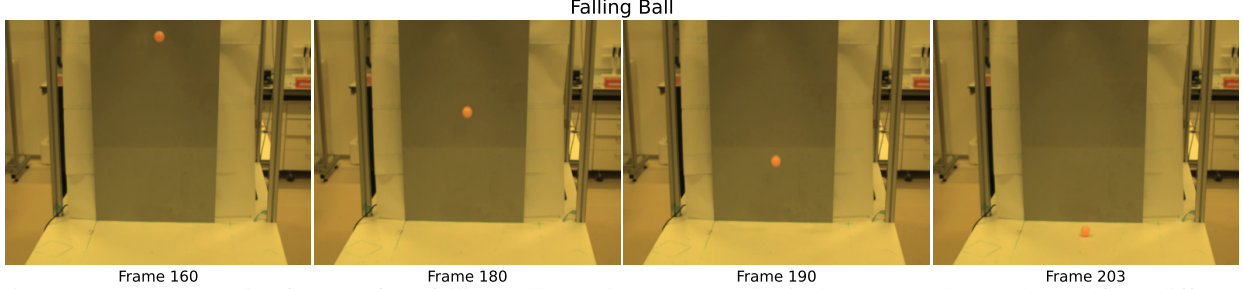


Figure A1: Representative frames of the falling ball experiment. A mechanical actuator releases the ball from different heights. The final frame of each sequence marks the exact moment the ball contacts the surface.

Bouncing ball The bouncing ball experiment begins immediately after the falling ball makes impact with the surface. It focuses on observing the ball during its bounce, capturing its trajectory as it rebounds upwards after contact with the surface.

Projectile For this experiment, a custom 3D printed projectile was built, along with three different balls of the same plastic material but of different colors. The projectile works with string rubber bands following the same principle of a slingback. During our recordings, we varied three different parameters. The angle of the launch for the ball, the force with which the ball was launched into the air, and the color of the ball.

Holonomic pendulum For this setting, a rigid metal structure consisting of a pole, perpendicular to the ground, on which a solid metal stick was mounted. The joint holding the stick was adjusted to allow for a normal friction coefficient, resulting in an intuitive retrogressive back-and-forth movement simulating a typical pendulum oscillatory trajectory. At the end of the metal stick a small table tennis ball was attached, as the SAM2 predictor can confidently track the center of the ball aligning with the central axis at the end of the stick. Using the zero angle as the resting

²Motor Model: T825, Motor serial number: 00362129

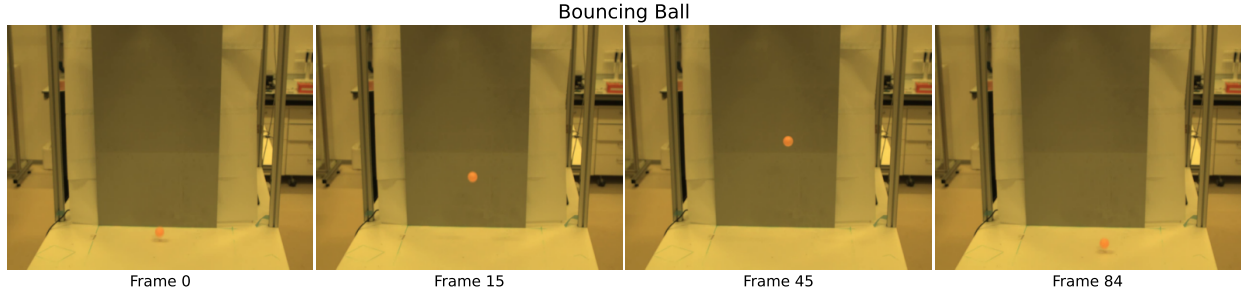


Figure A2: Representative frames of the bouncing ball experiment. A mechanical actuator releases the ball from different heights. This experiment begins immediately after the ball's initial contact with the surface and ends after the next touch.

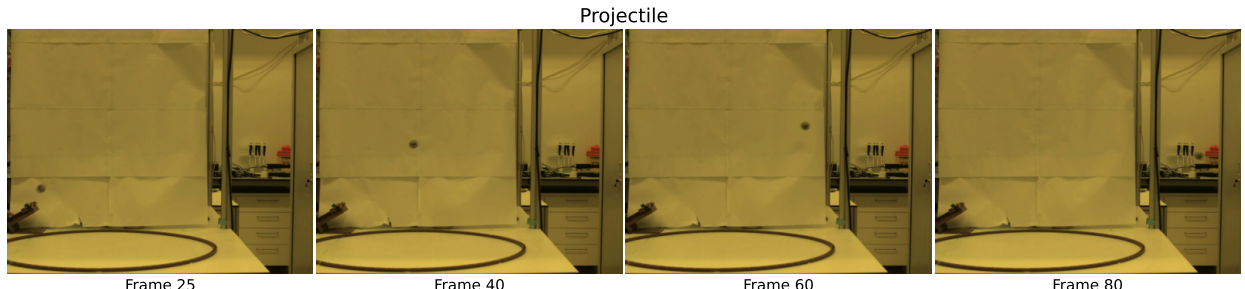


Figure A3: Representative frames of the projectile motion experiment with a 3D-printed launcher. In the dataset the launch angle, force, and ball color are varied.

position, we varied the angle at which the pendulum was released resulting in distinct retrogressive trajectories. As in the falling ball experiment the same release mechanism model was employed to manipulate the moment the pendulum was let freely to swing.

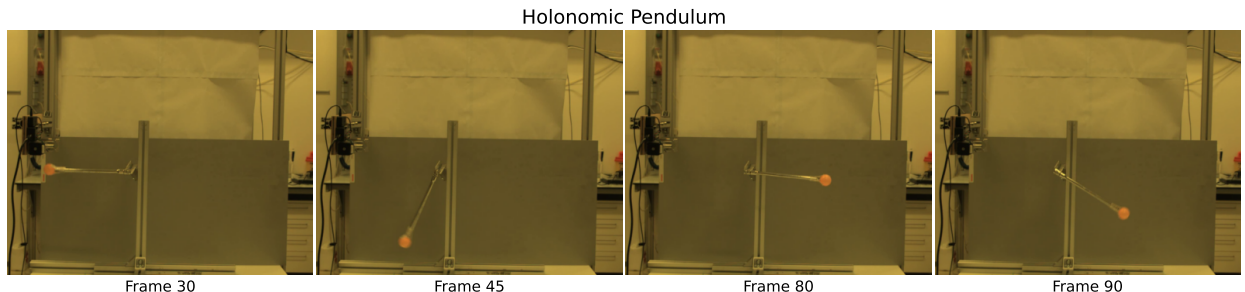


Figure A4: Representative frames of the holonomic pendulum experiment. The pendulum is released by a mechanical actuator and swings from varying starting positions, resulting in different initial angles.

Non-holonomic pendulum The setup for the non-holonomic pendulum is almost identical to that of the holonomic one, with the difference being that instead of a non-deformable metal structure, a flexible metal string was employed. The metal string on its top end had a noose so that it can be hanged from certain points, while at the other end, we attached a standard table tennis ball as in the holonomic pendulum case. Using the same release mechanism we can control the initial angular position with respect to the resting (vertical) position, at the very beginning of the trajectory, while the object is still stationary.

Double pendulum A custom structure consisting of a wooden base, a metal pole mounted on the top of the base, and a joint mounted at a degrees angle to the center axis of the pole, to keep the longer bob of the pendulum in place. These structures ensure that each 3D printed plastic bobs of the pendulum can rotate freely with normal friction resulting in the typical chaotic motion double pendulum are known for. A double pendulum consists of two bobs attached end-to-end. Each pendulum has its angle relative to the vertical. The same release mechanism as in previous experiments is utilized

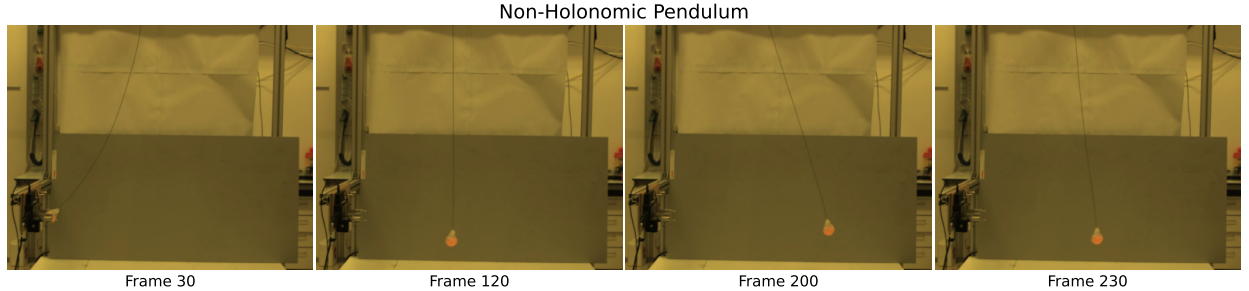


Figure A5: Representative frames of the non-holonomic pendulum experiment. A flexible metal string suspends a table tennis ball, with initial angles controlled by a mechanical actuator functioning as release mechanism.

to define the starting position of each pendulum link. This starting position can be described as the angle each bob makes with the vertical when it is still stationary.

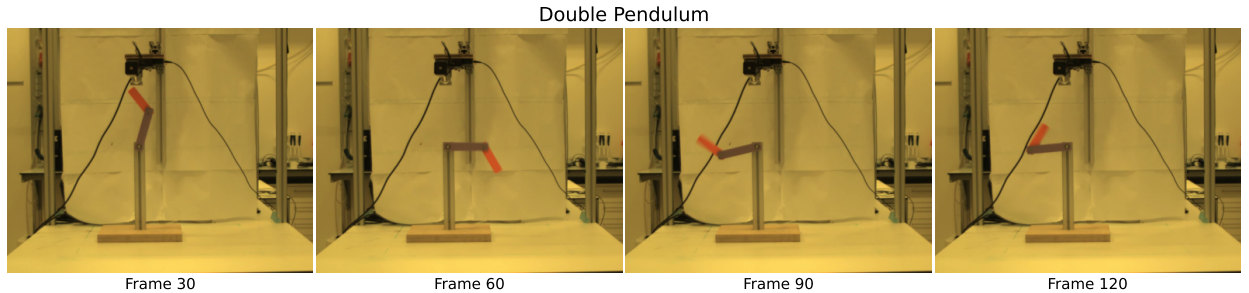


Figure A6: Representative frames of the double pendulum experiment. A custom-built structure with a metal pole and joint supports the 3D-printed plastic bobs, allowing for free rotation with minimal friction. The initial angles of both pendulum links are precisely controlled using a mechanical actuator.

B Velocity and acceleration estimation

We estimate objects' velocity and acceleration from the extracted trajectory using multiple stages.

We use the central difference method for most points in the time series. This method computes velocity by considering both forward and backward positions, reducing single-sided differentiation errors.

$$v_i = \frac{x_{i+1} - x_{i-1}}{t_{i+1} - t_{i-1}}, \quad 1 \leq i \leq N-2 \quad (\text{A1})$$

Since the central difference is not applicable at endpoints, we use one-sided differences. Forward difference (starting point):

$$v_0 = \frac{x_1 - x_0}{t_1 - t_0}$$

Backward difference (ending point):

$$v_N = \frac{x_N - x_{N-1}}{t_N - t_{N-1}}$$

To enhance precision, we perform linear regression within a sliding window.

$$x(t) = vt + b \quad (\text{A2})$$

The velocity (slope) is solved using the least squares method with window size w:

$$\begin{bmatrix} v \\ b \end{bmatrix} = (A^T A)^{-1} A^T x \quad (\text{A3})$$

where matrix A contains time information.

$$A = \begin{bmatrix} t_1 & 1 \\ t_2 & 1 \\ \vdots & \vdots \\ t_w & 1 \end{bmatrix} \quad (\text{A4})$$

We combine linear regression and central difference results using weighted averages.

$$v_{\text{final}} = \alpha v_{\text{regression}} + (1 - \alpha) v_{\text{central}} \quad (\text{A5})$$

Here $\alpha = 0.7$, indicating greater confidence in the regression method. Finally, we apply Savitzky-Golay filtering for smoothing [37]. This step effectively removes high-frequency noise from velocity calculations.

$$v_{\text{smoothed}} = \text{SG}(v_{\text{final}}, \text{window}, 3) \quad (\text{A6})$$

The entire calculation process can be summarized as:

$$v(t) = \text{SG}(\alpha v_{\text{regression}}(t) + (1 - \alpha) v_{\text{central}}(t), w, 3) \quad (\text{A7})$$

where w is the window size (odd number for symmetry); $\alpha = 0.7$ is the weighting coefficient; SG represents Savitzky-Golay filter of order 3; Regression window range: $[t - w/2, t + w/2]$.

For the acceleration, we first calculate the acceleration using the central difference. For $1 \leq i \leq N - 2$:

$$a_i = \frac{v_{i+1} - v_{i-1}}{t_{i+1} - t_{i-1}} \quad (\text{A8})$$

Dealing with the endpoints using the same metric as velocities, we get the final acceleration for the entire trajectory.

$$\begin{aligned} a_0 &= \frac{a_1 - a_0}{t_1 - t_0} \\ a_N &= \frac{v_N - v_{N-1}}{t_N - t_{N-1}} \end{aligned}$$

C Evaluation metrics

C.1 Discard rate

We generate N_{total} videos for each type of experiment. Among these videos, we discard those that do not meet our quality standards, following a three-stage filtering out. First, we discard videos where object are disappearing from the videos the number of such videos is $N_{\text{disappear}}$. Second, we analyze the number of objects in each video and discard videos that do not maintain a consistent object count in the not discarded yet videos. For this purpose we employ DEVA tracking [38] built on top of Grounded SAM [39] (with object names from the prompt as Grounding DINO [40] query) for consistent open-vocabulary prediction of 2D object masks. We denote the number of discarded videos in this step as $N_{\text{duplicate}}$. Specifically, we evaluate the proportion of frames containing multiple objects. Videos are filtered out if this proportion exceeds a predetermined threshold. Finally, we discard videos where the motion is too small to be meaningful in the not discarded yet videos, the number of such videos is N_{still} . The overall *discard rate* DR is defined as

$$DR = \frac{N_{\text{disappear}} + N_{\text{duplicate}} + N_{\text{still}}}{N_{\text{total}}}.$$

C.2 Depth Consistency Evaluation

In all the studied experiments, the video camera is orthogonal to the object’s motion and is fixed. This allows us to compute the Physical Invariance and Dynamical scores using only information extracted from 2D pixel space, available for generated videos. The results are presented in Fig. A7, showing that most of the models are reasonably consistent and thus object properties like energy conservation could be also studied using only 2D coordinates.

C.3 Physically-informed Neural Networks

Unlike typical neural networks, which are normally trained only on data, prior knowledge about the physical system is integrated into PINNs. This prior knowledge of the physical system, often in governing physical laws such as Newtonian mechanics or energy conservation, is imposed during training. Given that the system modeled from the

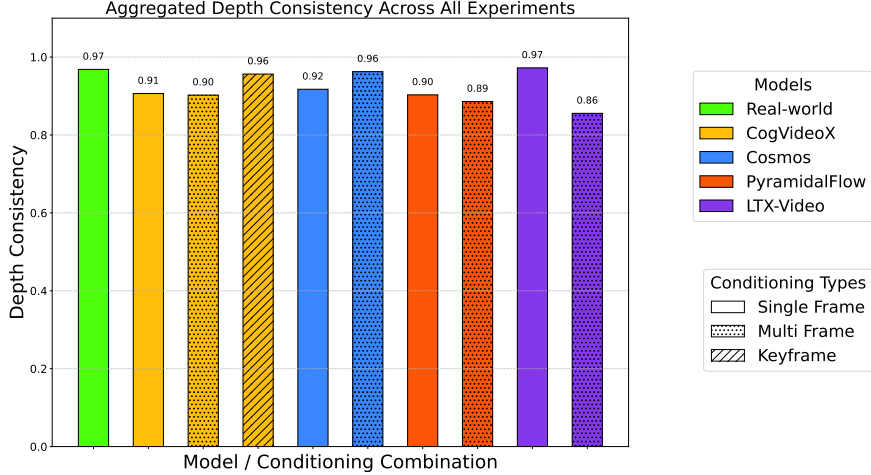


Figure A7: Average depth consistency for different video generation models across all studied experiments.

generated videos is known from the provided prompt, the training process incorporates these laws into the loss function. The total loss for a PINN is defined as:

$$L_{\text{total}} = L_{\text{data}} + \lambda L_{\text{physics}}, \quad (\text{A9})$$

where L_{data} ensures that the network's output can match the observed data. At the same time, L_{physics} is penalizing deviations from the governing physical equation and λ is a hyperparameter balancing the contribution of the each loss component. For our own experimentation λ has a value of 1. In this way, PINNs can bring both data and physical laws together during training while being consistent with the underline physical system. For a trajectory T , the data loss is defined as

$$L_{\text{data}} = \frac{1}{N} \sum_{i=1}^N \|\hat{T}_i - T_i\|^2, \quad (\text{A10})$$

, where \hat{T}_i is the trajectory predicted by the network at the i -th timestep and T_i is the corresponding ground truth trajectory at the same timestep. On the other hand, the physics loss is derived separately for each experiment, given the nature of the system's dynamics. The motion of a free-falling object follows:

$$\ddot{y} + g = 0, \quad (\text{A11})$$

where y is the vertical position, \ddot{y} is the acceleration and g is the gravitational constant. This means that for this phenomenon, the loss is defined as: The physics loss for free fall is defined as:

$$L_{\text{physics}} = \frac{1}{M} \sum_{j=1}^M \|\hat{y}_j + g\|^2, \quad (\text{A12})$$

where \hat{y}_j is the predicted acceleration derived from the PINN at the j -th time step. The motion of a holonomic pendulum is governed by:

$$\ddot{\theta} + \frac{g}{l} \sin \theta = 0, \quad (\text{A13})$$

where θ is the angular displacement, l is the pendulum length and g is the gravitational constant.

The corresponding physics loss is:

$$L_{\text{physics}} = \frac{1}{M} \sum_{j=1}^M \left\| \hat{\theta}_j + \frac{g}{l} \sin(\hat{\theta}_j) \right\|^2, \quad (\text{A14})$$

where $\hat{\theta}_j$ and $\hat{\theta}_j$ are the network-predicted angular acceleration and displacement, respectively, at the j -th timestep. In the present work, we use the Dynamical score to evaluate how well the does the predicted trajectories align with the ground truth. The Dynamical score is derived from the Normalized Mean Squared Error (NMSE), which provides a relative measure of error by normalizing the Mean Squared Error (MSE) with the variance of the ground truth trajectory. Main motivation behind this choice, is to make the evaluation independent of scale. The NMSE is calculated as:

$$\text{NMSE} = \frac{\frac{1}{N} \sum_{i=1}^N (y_i - \hat{y}_i)^2}{\frac{1}{N} \sum_{i=1}^N (y_i - \bar{y})^2}, \quad (\text{A15})$$

Table A2: Conserved quantities for each physical experiment in an ideal case.

Experiment Name	Assumption	Conserved Quantities
falling ball	no air resistance	energy, acceleration (gravity), horiz. momentum
projectile	no air resistance	energy, acceleration (gravity), horiz. momentum
bouncing ball	no air resistance	energy, acceleration (gravity), horiz. momentum
holonomic pendulum	low resistance	energy, period, pendulum length
non-holonomic pendulum	low resistance	energy (approximately)
double pendulum	low resistance	total energy, two pendulums length

where:

- y_i is the true value at timestep i ,
- \hat{y}_i is the predicted value at timestep i ,
- \bar{y} is the mean of the ground truth values, defined as:

$$\bar{y} = \frac{1}{N} \sum_{i=1}^N y_i, \quad (\text{A16})$$

- $\frac{1}{N} \sum_{i=1}^N (y_i - \hat{y}_i)^2$ represents the MSE between the predicted and ground truth trajectories,
- $\frac{1}{N} \sum_{i=1}^N (y_i - \bar{y})^2 = \sigma^2$ represents the variance of the ground truth trajectory.

To ensure robustness, the predicted trajectory is compared against the interpolated ground truth values. Depending on the experiment, we address physical consistency by quantifying how well the learned solution adheres to the underlying physical equation. This is quantified using the physics loss, which penalizes deviations from the expected dynamics. For training, each PINN is optimized using the Adam optimizer with a learning rate of 10^{-3} for 200,000 iterations. The network used for all experiments, consists of two hidden layers of 20 neurons, with tanh as activation functions. The final score is defined as $S_{dyn} = \min(1 - \text{NMSE}, 0)$. Similarly to the Physical Invariance score, in cases when the original trajectory is discarded, the score is assigned to a minimal value equal to zero.

C.4 Physical Invariances

Falling Ball For falling balls, energy must be conserved between consecutive bouncing points. Additionally, according to Newton's second law:

$$F = ma$$

In free fall, gravity is the sole force acting on the object, resulting in constant acceleration. Assuming that the gravitational field is uniform in space and time, we have $F = mg$, which means that $a = g$, so the acceleration should stay constant. Therefore, in this part, we introduce three quantitative metrics to assess trajectory physics: the Energy Conservation score (ES), which measures energy conservation within a specified time window, and the Acceleration Conservation score (AS), which evaluates the consistency of acceleration during this interval, and the Horizontal Momentum Conservation score (MS), which measures the conservation of momentum.

The Energy Conservation score is calculated as follows. Given the mass of the ball to be m , the g a freefall acceleration constant, kinetic energy:

$$T = \frac{1}{2}m|\vec{v}|^2 = \frac{1}{2}m(v_x^2 + v_y^2)$$

and potential energy:

$$V = mgh$$

where $h = y$. Total energy is the sum of two:

$$E = T + V = \frac{1}{2}m(v_x^2 + v_y^2) + mgy$$

From this formula, assuming the mass of the ball is constant in time, we get:

$$\frac{E}{m} = \frac{1}{2}(v_x^2 + v_y^2) + gy = \text{const} \quad (\text{A17})$$

The calculation of the Acceleration Conservation score is self-evident:

$$a = \text{const} \quad (\text{A18})$$

The conservation of horizontal momentum arises from the fact that the only force acting on the ball is gravity, which is pointed downwards:

$$p_x = mV_x = \text{const}$$

and analogous to the energy, we deduce:

$$\frac{p_x}{m} = V_x = \text{const} \quad (\text{A19})$$

We provide some examples of estimated invariants in Fig. A8

Projectile For projectile motion, we analyze the same physical invariants as in the falling ball experiment. Throughout the projectile's trajectory, neglecting the air resistance, energy, acceleration, and horizontal momentum should be conserved. The calculations for energy and acceleration follow the same methodology used in the falling ball analysis.

Holonomic Pendulum For the holonomic pendulum, let's first examine energy conservation. Energy in the ideal (frictionless) case:

$$H = T + V = \frac{p_\theta^2}{2mL^2} + mgL(1 - \cos \theta)$$

where θ is the angular displacement, l is the pendulum length, g is the gravitational acceleration, and $p_\theta = mL^2\dot{\theta}$ is the momentum.

In this case, the equation that we obtain is:

$$\ddot{\theta} + \frac{g}{l} \sin \theta = 0$$

Since our real-world pendulum experiments were conducted in a laboratory environment, friction causes energy attenuation over time. We quantify this energy loss by measuring both its range and rate of decline, establishing these as upper bounds for evaluating generated videos. To be specific, the holonomic pendulum with friction can be expressed as

$$\ddot{\theta} + \frac{b}{m}\dot{\theta} + \frac{g}{l} \sin \theta = 0 \quad (\text{A20})$$

where b is the damping coefficient, m is the bob mass, and $\frac{b}{m}\dot{\theta}$ represents the damping force term. The energy decay over time:

$$\frac{dE}{dt} = -b(\dot{\theta})^2 \quad (\text{A21})$$

In our experiments, we assume that the energy loss can be ignored for a short time period, meaning we can apply the Energy Conservation score.

The period of holonomic pendulum with friction with a small amplitude can be expressed as

$$T = 2\pi \sqrt{\frac{l}{g}} \sqrt{1 - \left(\frac{b}{2m\omega_0}\right)^2} \quad (\text{A22})$$

where $\omega_0 = \sqrt{\frac{g}{l}}$ is the natural angular frequency without damping. When the damping is small ($b \ll m\omega_0$), the period approaches that of an undamped pendulum $T_0 = 2\pi\sqrt{\frac{l}{g}}$. We observe this regime in our experiments and propose to use the Period Conservation score (PC).

For the holonomic pendulum, it is obvious that the pendulum length l remains constant throughout the experiment, as the holonomic constraint of the system. Therefore, we also consider the pendulum length as a physical invariant.

Non-holonomic Pendulum For an ideal non-holonomic pendulum, energy conservation holds since non-holonomic constraints only restrict possible paths without energy dissipation. However, in laboratory conditions, the suspension string's deformation and friction cause some energy decay. As with the holonomic pendulum case, we measure this energy decay range in real-world videos and use it to evaluate generated videos.

Since both period and pendulum length vary in non-holonomic pendulums, we exclude these metrics from our analysis, keeping only the energy.

C.5 Physical Score Scaling

When we obtain the physical invariant value C , we calculate the relative standard deviation over time:

$$C_{\bar{\sigma}} = C_{\sigma}/C_{mean} \quad (\text{A23})$$

To ensure that the score is within the $[0, 1]$ range, we design the Physical score, derived from the invariant, as follows

$$S = \frac{1}{1 + \alpha * C_{\bar{\sigma}}} \quad (\text{A24})$$

Where α is a normalization factor. In the experiment, we set it to 1.0.

Two critical considerations emerge during the score calculation process. First, The time window must be carefully selected. For each trajectory, we partition it using a sliding time window and select the highest score among all segments as the trajectory's overall score. This approach addresses a key challenge in real-world experiments like bouncing balls, where fluctuations near bouncing points create large standard deviations and low scores. By using the highest score across all segments, we effectively capture the most stable portion of the trajectory.

In our experiments, we set the time window length between 10% and 25% of the total trajectory duration. Specifically, for real videos, we use $t_{window} = L_{trajectory}/10$, while for generated videos, we use $t_{window} = L_{trajectory}/4$. This difference in window size is necessary because generated videos have much shorter total durations - using $t_{window} = L_{trajectory}/10$ would result in trajectory segments that are too short for meaningful analysis.

Second, proper scaling is essential: since the trajectory coordinates are recorded in pixel space rather than real-world 3D coordinates, a precise coordinate transformation to physical units is required. Notably, improper scaling can significantly impact the total energy calculations. Third, we need to be careful not to choose the range when the mean of the selected physical invariant is near zero. The absolute value of mean of the selected physical invariant should be equal to or greater than a threshold of 10 times of standard deviation:

$$C_{threshold} = 10 * C_{\sigma} \quad (\text{A25})$$

so it can be neglected that the influence of mean energy/acceleration is near zero. In the experiment, if $|C_{mean}| \geq C_{threshold}$, we calculate the Physical score as defined in Eq. A24. Otherwise, we use the following Eq. A26 that takes the absolute standard deviation rather than the relative standard deviation.

$$S = \frac{1}{1 + \alpha * C_{\sigma}} \quad (\text{A26})$$

This method has two key limitations. First, the scores are highly sensitive to the choice of time window size. Larger time windows tend to yield lower scores as they encompass more fluctuations in the trajectory. Second, the method may fail to detect unphysical behavior in generated videos where objects remain stationary for long periods. Since we only consider the highest score among all segments, these periods of stillness - which would receive low scores - are effectively ignored in our evaluation. In future work, we plan to introduce a penalty term to specifically address and discourage such unphysical stillness behavior.

D Video Generative Models Details

At their core, latent video generative models often utilize a combination of a 3D Variational Autoencoder (VAE) [41, 42] to tokenize individual frames, a text encoder, like T5 [43] to encode frames into latent. During training a noisy latent is produced by the forward diffusion process. This latent is then processed by a parametrized model, either a transformer model [44] or a U-Net [45, 46, 47] resulting in a patchified long sequence of visual tokens, in case of the former type of model.

Depending on the model architecture different input modalities can be handled like text-to-video, image-to-video, text+image-to-video, and sometimes video continuation regimes facilitating both open-domain and controlled generation scenarios [16, 48, 5, 49]. Although some state-of-the-art video generation models adopt an autoregressive framework, predicting frames sequentially based on prior outputs [50, 51, 52], many others utilize non-autoregressive approaches to generate frames simultaneously [16, 48, 53]. In Table A3, we specify the parameters of particular models used in our benchmark, along with its architectural design choices. As to faithfully get the best generation outcome we use the best hyperparameters reported for each model. Due to the high API costs-per five seconds video, along with the impressive performance of COSMOS [5] among established benchmarks, we opted to not use any closed-source VGMs like [7, 54]. Still all the open-source alternatives used for our analysis match the performance of most closed-source one across established benchmarks for VGMs.

Model	Category	Resolution	Number of Video Frames	Guidance Scale	Sampling Steps
CogVideoX	single-frame generation	960 x 768	84	6.0	50
Cosmos	single-frame generation	1280 x 704	121	7.0	35
LTX-Video	single-frame generation	960x736	81	3.0	50
PyramidalFlow	single-frame generation	1280 x 768	121	4.0	10

Table A3: Details of video generation models adopted in our benchmark study, including their category, resolution, number of video frames, guidance scale, and sampling steps.

E Prompts for Video Generation Models

For each experiment, we carefully designed a prompt that describes the physical setup and motion of the experiment being conducted. For example, in the falling ball experiment, the prompt specifies that the ball falls and makes contact with the table below. Similarly, in the projectile experiment, we describe how the ball is launched at a slight upward angle and follows a natural parabolic trajectory. We enhance these prompts using ChatGLM to incorporate more detailed scene descriptions and contextual elements derived from the reference images. All prompts are shown in Table A4,

F Additional Analysis

In Figure A8 we present additional visualization of the energy and acceleration conversation. In Figure A9 and Figure 9 we visualize difference between real-world and generated videos object trajectories.

F.1 Falling ball

In Figure A8 (a), we present the total, kinetic, and potential energy over time. As expected, the total energy dissipates with every new bounce while remaining nearly constant between bounces. Per the video generation method, the discard rate ranges from 11% for COSMOS with enhanced text prompts up to 77% for CogVideoX in a single-frame conditioning regime with plain prompt. The best Dynamical score is achieved by the COSMOS model of 0.35, which is, however, still far from the real-world video score (0.99). Physical invariance scores range from 0.149 (CogVideoX, single-frame, plain text prompt) to 0.582 (PyramidalFlow, multi-frame, plain text prompt). We notice that enhanced text prompts increase the scores for COSMOS and CogVideoX, but reduce it for LTX and PyramidalFlow. The qualitative analysis of the discard reasons in Fig. A12 (upper) provides the clue for the low scores, i.e. the overall abundance of duplicates in the videos, as well as the lack of motion. The qualitative inspection of falling and bouncing ball (Fig. A8, c-d) supports this claim. In the case of CogVideoX, generated videos partially exhibit the *stillness problem*, characterized by an initial absence of motion followed by abrupt and chaotic movements, which deviate significantly from realistic physical behavior.

F.2 Bouncing ball

The main results for the bouncing ball are presented in Tab. A6. Real-world videos achieve optimal performance, reflected by a minimal Discard Rate (0.0), a high Dynamical score (0.99), and a high Physical Invariance score (0.99). In contrast, generated videos display notably lower physical invariance scores, especially evident in plain prompts. The discard rates, presented in Fig. A12 (lower) are lower on average compared to other experiments. Among single-frame methods, COSMOS (enhanced) achieves the highest physical invariance score (0.546) but still falls substantially below the real-world baseline. Multi-frame methods generally exhibit improved dynamical and physical scores compared to their single-frame counterparts, although their overall scores remain significantly below those of real-world videos. The first and last frame conditioning with plain prompts surprisingly shows slightly better performance (Physical Invariance score of 0.587) compared to the enhanced version (0.550).

F.3 Projectile

In the case of the projectile, we present the main results in Tab. A7. As for generated videos, the Discard Rates seem to have the same range as for the falling ball, with the main reasons for discarding being the presence of duplicate objects and stillness (see Fig. A12 (middle)), though the disappearance now exhibiting more often, e.g. LTX multi-frame with enhanced prompting. Though the Dynamical and Physical Invariance scores seem 10% lower for the real-world videos compared to other experiments, they are still unreachable for other models.

Experiment Name	Base Prompt	Enhanced Prompt
Falling Ball	Orange ping-pong ball falling down and making impact with the table surface below. Fixed camera view, no camera movement.	A ping-pong ball is captured in mid-air, suspended above a laboratory table, poised to make contact with the surface below. The ball's descent is governed by the force of gravity, creating an arc that suggests a controlled experiment in progress. The backdrop is a stark, clinical room with a neutral palette, punctuated by the sterile lines of a metal frame and the functional design of a nearby cabinet. The lighting is subdued, casting a soft glow that highlights the ball's trajectory and the anticipation of impact. The table beneath the ball is marked with faint lines, perhaps indicating measurements or guidelines for the experiment. As the ball continues its downward journey, it will likely bounce off the table, adding a dynamic element to the scene and marking the conclusion of this controlled descent. Fixed camera view, no camera movement.
Bouncing Ball	A single orange ping pong ball bounces vertically as a result of making impact with the table after being in free fall. The ball starts in the center of the frame, and moves upwards. Fixed camera view, no camera movement.	A solitary orange ping pong ball, with its vibrant hue standing out against the stark white of the table, plummets from the center of the frame. As the ball bounces upwards, it arcs gracefully, the trajectory a perfect parabola. The frame remains centered, emphasizing the ball's solitary dance of motion and the physics of its rebound. Fixed camera view, no camera movement.
Projectile	A single, small 3D-printed ball, dark gray in color, is launched from a plastic, small-scale ramp with a slight upward angle. The ball follows a natural, smooth, arcing trajectory upward and then downward, continuing along that arc until it exits the right side of the video frame. The video should accurately simulate the ball's motion under standard Earth gravity, showing a clear parabolic arc. The ball should not bounce or collide with any objects in the scene. Fixed camera view, no camera movement.	In a meticulously crafted scene, a solitary, dark gray 3D-printed ball, with its sleek, spherical form, is propelled from a plastic ramp that slopes gently upward. The ball, weighing a mere fraction of a kilogram, is captured in high-definition, showcasing every nuance of its motion. As it leaves the ramp's edge, the ball arcs gracefully into the air, its trajectory a perfect parabola that mirrors the laws of physics under standard earth gravity. The video's frame follows the ball's smooth ascent and descent, highlighting the ball's consistent speed and the absence of any sudden accelerations or decelerations. The scene remains unobstructed, ensuring that the ball's journey is uninterrupted by any external forces, save for the pull of gravity, resulting in a visually stunning and scientifically accurate demonstration of a parabolic motion. Fixed camera view, no camera movement.
Holonomic Pendulum	A single pendulum moving retrogressive back and forth. At the bottom of the pendulum, there is a ball attached to it. The pendulum is holonomic. Fixed camera view, no camera movement.	A pendulum with a spherical ball attached swings back and forth in a controlled manner, its motion captured in a moment of retrograde swing. The pendulum's arm, likely made of metal, extends horizontally from a stand, connected to a pivot point that allows for rotational movement. The ball, positioned at the lower end of the pendulum, appears to be in motion, indicating the pendulum's swing. The environment suggests a laboratory or testing setting, with a backdrop of technical apparatus and equipment, and the lighting is artificial, casting a uniform glow over the scene. The pendulum's movement, while currently in a retrogressive swing, could potentially change direction, continuing its oscillatory motion. Fixed camera view, no camera movement.
Non-Holonomic Pendulum	A single pendulum swings smoothly back and forth. The pendulum consists of a thin, dark string, and at the bottom of the string, there is a small orange ball. The motion of the pendulum is realistic, with slowing at the peaks of its arc and accelerating through the center, simulating gravity's effect. The pendulum is non-holonomic, so its swing is not perfectly planar, and there might be small, natural deviations in its path. Fixed camera view, no camera movement.	In high-definition clarity, a solitary pendulum gracefully arcs through the air, its thin, dark silk string coiling and uncoiling with each oscillation. At the string's terminus, a small, vibrant orange ball swings with a life-like fluidity, its trajectory punctuated by the subtle slowing at the zenith of its arc and the swift acceleration as it crosses the midpoint. The pendulum's non-holonomic nature is evident, as it sways slightly off-axis, revealing the gentle, imperceptible wobble that mimics the real-world influence of gravity. Fixed camera view, no camera movement.
Double Pendulum	Double pendulum, consisting of a purple and an orange segment. Each segment moves independently. Fixed camera view, no camera movement.	In a meticulously arranged laboratory setting, a double pendulum setup swings gracefully, each pendulum segment adhering to the immutable laws of physics. The upper pendulum, a sleek purple rod, contrasts strikingly with the lower orange rod, both suspended from a sturdy, metallic frame. The room is bathed in soft, ambient light, casting subtle shadows that accentuate the pendulums' arcs. The scene captures the intricate dance of the pendulums, their movements a mesmerizing testament to the natural order, with each swing a silent symphony of motion and balance. Fixed camera view, no camera movement.

Table A4: Base and enhanced textual prompts used for video generation experiments. Enhanced prompts are generated using ChatGLM [31]

and incorporate more detailed scene descriptions and contextual elements derived from the reference images.

F.4 Holonomic pendulum

We present the main results in Tab. A8. Real-world videos achieve near-perfect Dynamical (0.99) and Physical Invariance (0.94) scores, confirming our expectation that a real holonomic pendulum demonstrates consistent, physically accurate periodic motion. The discard rates vary considerably, from as low as 0% for first&frame CogVideoX (enhanced prompts) to as high as 92% for single-frame LTX with enhanced prompts (mainly due to the lack of motion, see Fig. A13 (upper)), indicating severe reliability issues for certain models. Multi-frame configurations tend to outperform single-frame models, achieving higher Dynamical and Physical Invariance scores, with COSMOS (multi-frame, enhanced) and PyramidalFlow (multi-frame, enhanced) showing strong relative performance. Additionally, CogVideoX using the first&last frame conditioning achieves notably high Dynamical scores (0.85), though still below the real-world benchmark. Despite capturing some periodic characteristics, the generated methods remain significantly below real-world realism, both quantitatively and qualitatively, suggesting substantial limitations in their ability to accurately model simple pendulum dynamics.

F.5 Non-holonomic pendulum

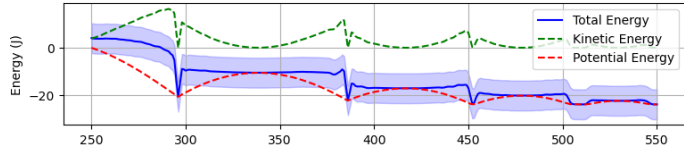
We present the main results for the non-holonomic pendulum experiment in Tab. A9. The real-world videos achieve near-ideal performance, indicated by a minimal discard rate (0.000), a high Dynamical score (0.98), and an excellent Physical Invariance score (0.996), validating that even non-holonomic pendulum motion adheres closely to expected physical invariants. Generated videos exhibit variable performance. Discard rates are generally lower compared to the holonomic pendulum scenario, suggesting that non-holonomic pendulum dynamics might be somewhat easier for generative models to approximate. CogVideoX, especially in multi-frame setups, demonstrates low discard rates (as low as 0.03) and high Dynamical scores (up to 0.86), indicating it can better capture some periodic characteristics of the pendulum. Nevertheless, Physical Invariance scores remain considerably below real-world performance, with the highest being 0.687 for single-frame COSMOS with plain prompts. Qualitative inspections (Fig. A9) further confirm that while periodic motion patterns, responsible for high Dynamical scores, are partially reproduced, the generated trajectories still significantly deviate from realistic physical behaviors in terms of energy conservation.

F.6 Double pendulum

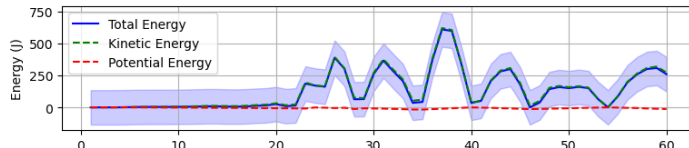
We present the main results for the double pendulum experiment in Tab. A10. Real-world videos achieve near-perfect Dynamical (0.99) and high Physical Invariance scores (0.938), serving as a robust benchmark and validating our expectations of minimal dynamical error and strong adherence to physical invariance. Generated videos achieve relatively high Dynamical scores, with the best synthetic performance being 0.94 (single-frame PyramidalFlow plain prompt). The discard rates vary significantly, from an ideal 0.0% for COSMOS (single-frame, plain) to as high as 77.8% for LTX (single-frame, enhanced), highlighting considerable variability among methods. Despite relatively strong Dynamical scores (up to 0.94), even the best-performing models show non-negligible dynamical errors (NMSE of 0.06 compared to the real-world NMSE of 0.002). The high Dynamical score but low Physical Invariance score may indicate plausible periodic-like motion, but no adherence to the actual physics, see Fig. 9.

F.7 Plain vs. enhanced text prompting

Enhanced text prompting consistently leads to a marked reduction in the discard rate across nearly all experiments and models (e.g., Fig. 6), indicating that the relevance of the generated videos strongly depends on model prompting. However, the gains in terms of the other scores are mixed. We can see that the difference varies from model to model and experiment to experiment, either increasing or decreasing the score or does not provide any significant changes.



(a)



(b)

Figure A8: Energy analysis of real-world and generated falling + bouncing ball videos: (a) Real-world video energy conservation (b) CogVideoX plain single frame generated video energy conservation

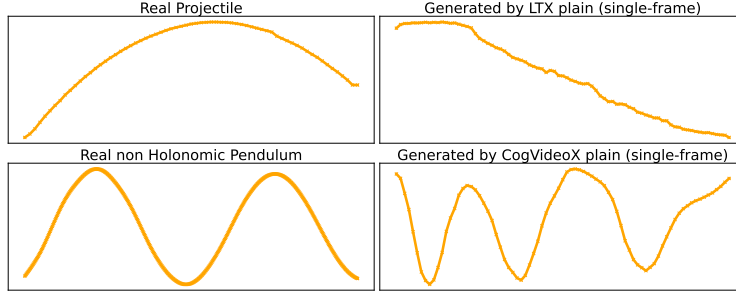


Figure A9: Real (left) vs. generated (right) for projectile (upper) and non-holonomic pendulum (lower).

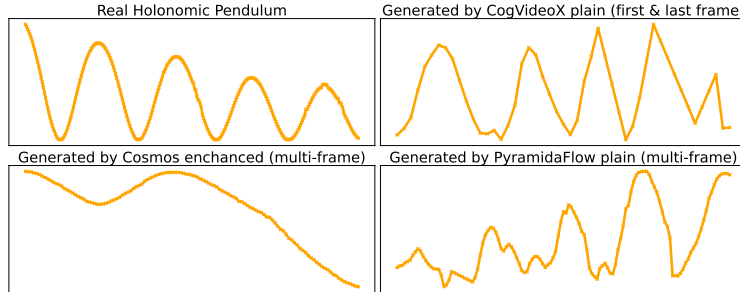


Figure A10: Real (top left) and generated trajectories for the holonomic pendulum.

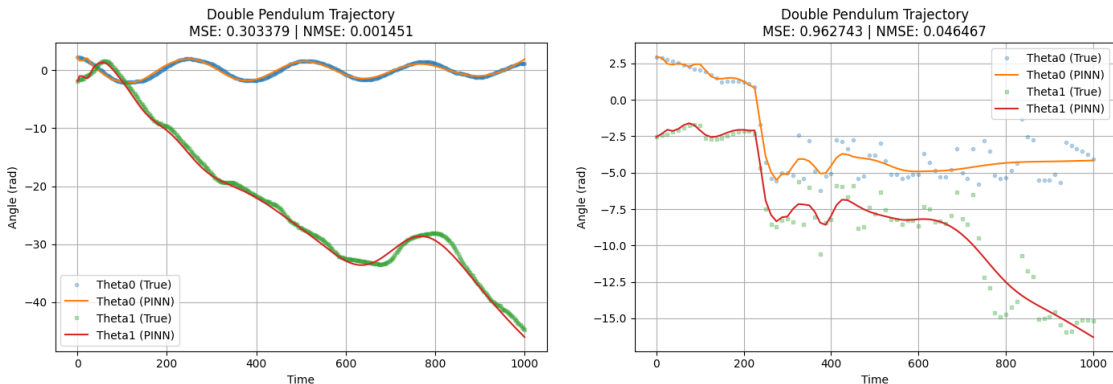


Figure A11: Real (left) and generated trajectory (right) for the double pendulum and corresponding fitting curve with PINN. While NMSE for generated trajectory is small 0.05, it is still 50 times worse than PINN with the same parameters fitted to real-world trajectory.

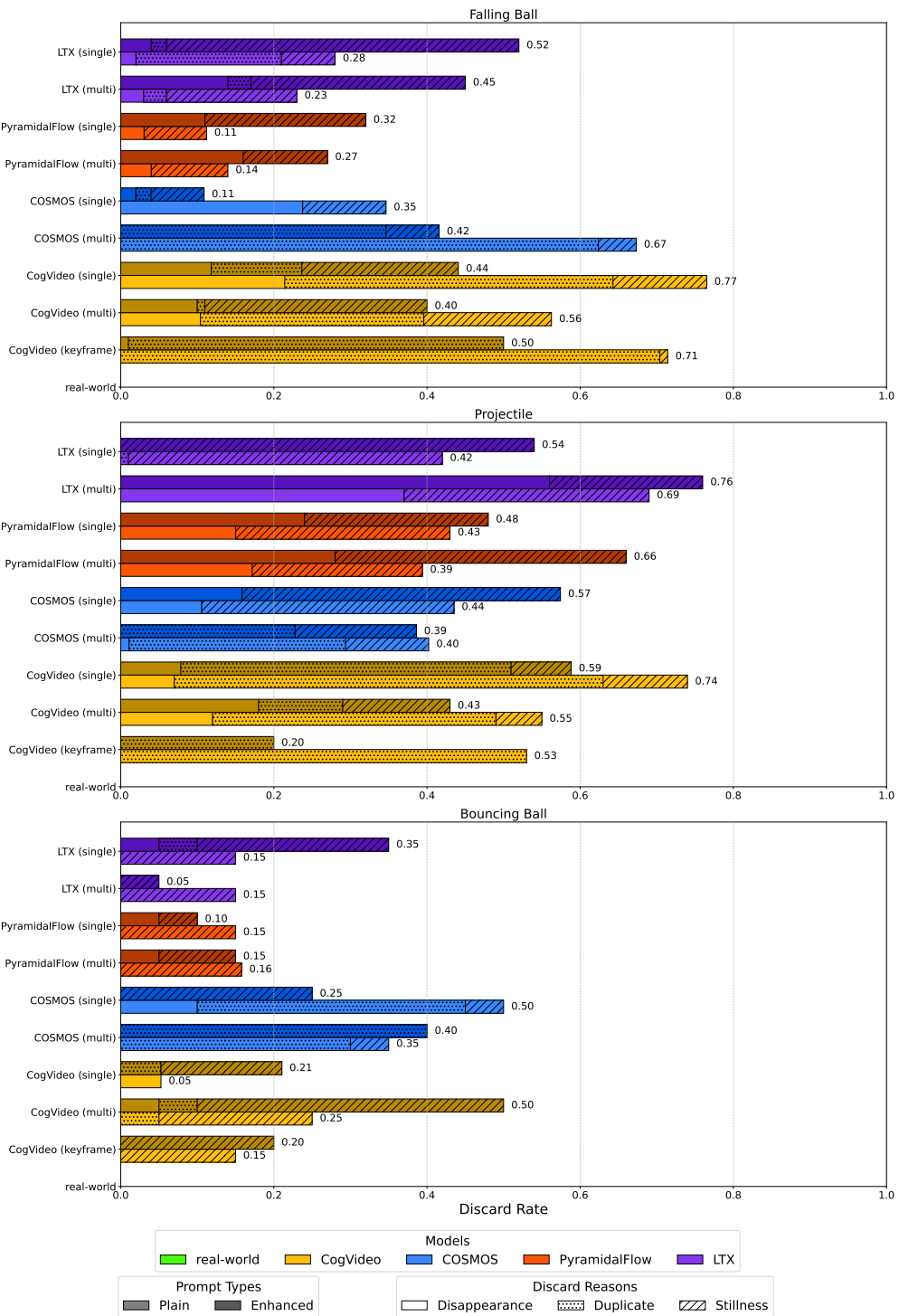


Figure A12: Discard rate reasons for Falling Ball, Projectile and Bouncing Ball experiments

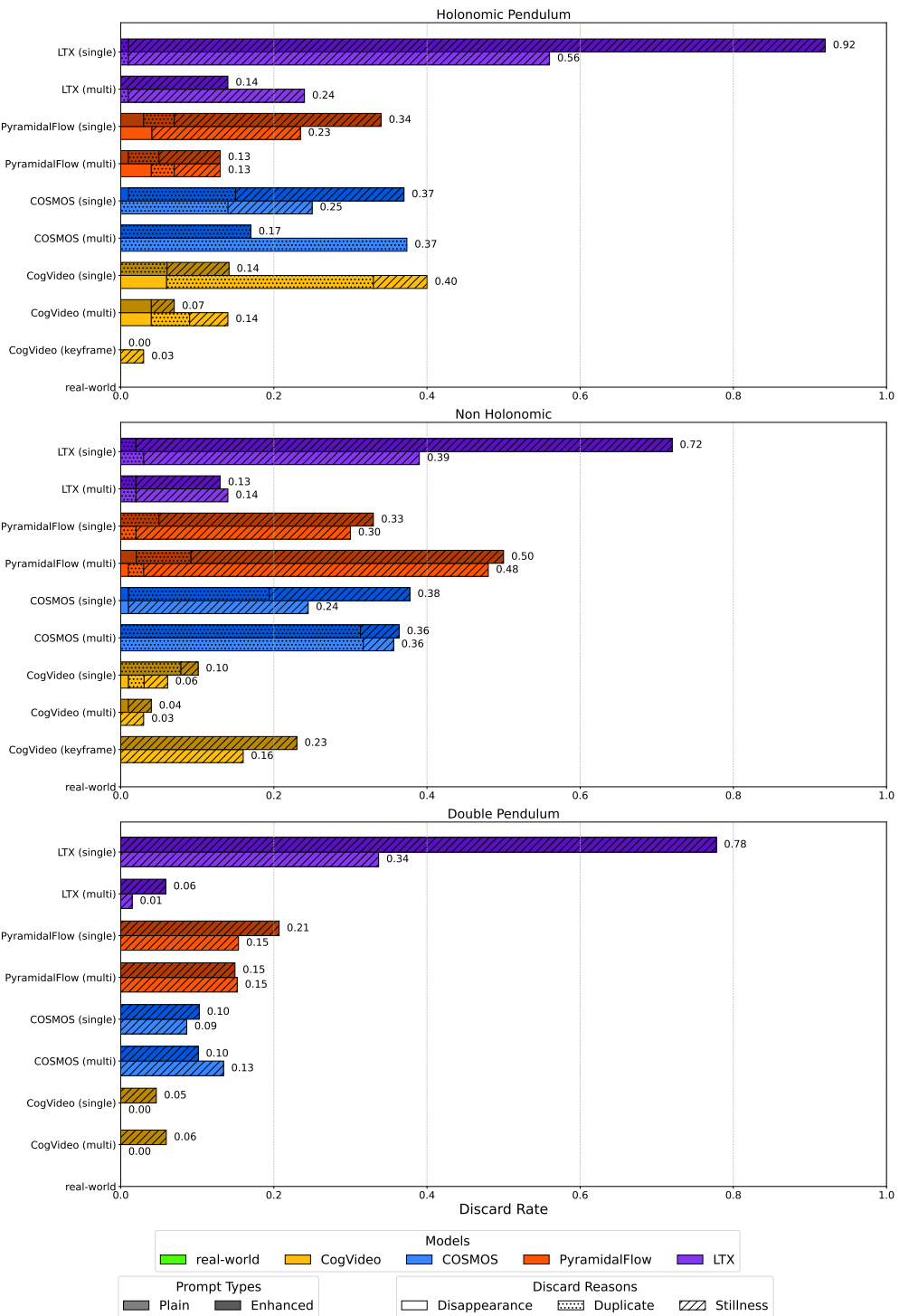


Figure A13: Discard rate reasons for Pendulum experiments

Experiment Name	Categories	Prompt Type	Discard Rate(\downarrow)	Dynamical Score(\uparrow)	Physical Invariance Score(\uparrow)	Energy Conservation(\uparrow)	Acceleration Conservation(\uparrow)	Horizontal Momentum Conservation(\uparrow)
real-world	real-world video	-	0.000	0.99	0.977	0.993	0.946	0.994
COSMOS	single-frame	enhanced	0.109	0.35	0.547	0.617	0.281	0.742
COSMOS	single-frame	plain	0.347	0.25	0.369	0.417	0.204	0.485
CogVideo	single-frame	enhanced	0.441	0.12	0.370	0.387	0.245	0.477
CogVideo	single-frame	plain	0.765	0.05	0.149	0.149	0.102	0.195
LTX	single-frame	enhanced	0.520	0.09	0.392	0.423	0.295	0.459
LTX	single-frame	plain	0.280	0.29	0.447	0.470	0.314	0.556
PyramidalFlow	single-frame	enhanced	0.320	0.26	0.491	0.587	0.299	0.586
PyramidalFlow	single-frame	plain	0.112	0.18	0.569	0.669	0.358	0.678
COSMOS	multi-frame	enhanced	0.416	0.20	0.395	0.447	0.202	0.535
COSMOS	multi-frame	plain	0.673	0.14	0.233	0.269	0.131	0.299
CogVideo	multi-frame	enhanced	0.400	0.21	0.457	0.463	0.337	0.572
CogVideo	multi-frame	plain	0.562	0.12	0.320	0.344	0.226	0.390
LTX	multi-frame	enhanced	0.450	0.18	0.371	0.389	0.243	0.480
LTX	multi-frame	plain	0.230	0.26	0.444	0.478	0.281	0.573
PyramidalFlow	multi-frame	enhanced	0.270	0.22	0.511	0.567	0.307	0.659
PyramidalFlow	multi-frame	plain	0.140	0.34	0.582	0.629	0.381	0.736
CogVideo	first&last frame	enhanced	0.500	0.13	0.372	0.371	0.308	0.437
CogVideo	first&last frame	plain	0.714	0.07	0.220	0.230	0.175	0.255

Table A5: Discard Rate, Dynamical score, Physical Invariance score, and Conservation metrics for Falling Ball

Experiment Name	Categories	Prompt Type	Discard Rate(\downarrow)	Dynamical Score(\uparrow)	Physical Invariance Score(\uparrow)	Energy Conservation(\uparrow)	Acceleration Conservation(\uparrow)	Horizontal Momentum Conservation(\uparrow)
real-world	real-world video	-	0.000	0.99	0.985	0.991	0.975	0.990
COSMOS	single-frame	enhanced	0.250	0.05	0.546	0.672	0.272	0.693
COSMOS	single-frame	plain	0.500	0.17	0.276	0.321	0.162	0.346
CogVideo	single-frame	enhanced	0.211	0.05	0.457	0.546	0.222	0.605
CogVideo	single-frame	plain	0.053	0.12	0.509	0.554	0.228	0.744
LTX	single-frame	enhanced	0.350	0.06	0.333	0.367	0.198	0.434
LTX	single-frame	plain	0.150	0.07	0.463	0.534	0.211	0.642
PyramidalFlow	single-frame	enhanced	0.100	0.11	0.663	0.789	0.382	0.819
PyramidalFlow	single-frame	plain	0.150	0.13	0.602	0.648	0.375	0.782
COSMOS	multi-frame	enhanced	0.400	0.35	0.362	0.341	0.229	0.516
COSMOS	multi-frame	plain	0.350	0.35	0.368	0.345	0.229	0.529
CogVideo	multi-frame	enhanced	0.500	0.11	0.331	0.335	0.237	0.422
CogVideo	multi-frame	plain	0.250	0.00	0.387	0.397	0.163	0.600
LTX	multi-frame	enhanced	0.050	0.12	0.476	0.532	0.265	0.630
LTX	multi-frame	plain	0.150	0.04	0.370	0.405	0.150	0.554
PyramidalFlow	multi-frame	enhanced	0.150	0.17	0.622	0.641	0.468	0.758
PyramidalFlow	multi-frame	plain	0.158	0.13	0.620	0.663	0.439	0.757
CogVideo	first&last frame	enhanced	0.200	0.22	0.550	0.537	0.498	0.614
CogVideo	first&last frame	plain	0.150	0.26	0.587	0.567	0.461	0.733

Table A6: Discard Rate, Dynamical score, Physical Invariance score, and Conservation metrics for Bouncing Ball

Experiment Name	Categories	Prompt Type	Discard Rate(\downarrow)	Dynamical Score(\uparrow)	Physical Invariance Score(\uparrow)	Energy Conservation(\uparrow)	Acceleration Conservation(\uparrow)	Horizontal Momentum Conservation(\uparrow)
real-world	real-world video	-	0.000	0.83	0.862	0.928	0.705	0.952
COSMOS	single-frame	enhanced	0.574	0.31	0.276	0.327	0.139	0.362
COSMOS	single-frame	plain	0.435	0.31	0.308	0.382	0.148	0.393
CogVideo	single-frame	enhanced	0.588	0.31	0.251	0.319	0.164	0.269
CogVideo	single-frame	plain	0.740	0.18	0.134	0.180	0.087	0.135
LTX	single-frame	enhanced	0.540	0.41	0.401	0.458	0.291	0.454
LTX	single-frame	plain	0.420	0.52	0.500	0.571	0.371	0.559
PyramidalFlow	single-frame	enhanced	0.480	0.43	0.410	0.470	0.282	0.479
PyramidalFlow	single-frame	plain	0.430	0.44	0.410	0.479	0.275	0.476
COSMOS	multi-frame	enhanced	0.386	0.30	0.350	0.382	0.209	0.460
COSMOS	multi-frame	plain	0.402	0.28	0.297	0.305	0.178	0.407
CogVideo	multi-frame	enhanced	0.430	0.38	0.273	0.354	0.199	0.267
CogVideo	multi-frame	plain	0.550	0.28	0.227	0.280	0.180	0.220
LTX	multi-frame	enhanced	0.760	0.19	0.150	0.165	0.118	0.168
LTX	multi-frame	plain	0.690	0.22	0.168	0.190	0.129	0.186
PyramidalFlow	multi-frame	enhanced	0.660	0.17	0.232	0.280	0.140	0.277
PyramidalFlow	multi-frame	plain	0.394	0.34	0.400	0.459	0.255	0.484
CogVideo	first&last frame	enhanced	0.200	0.61	0.506	0.542	0.335	0.640
CogVideo	first&last frame	plain	0.530	0.35	0.275	0.301	0.188	0.334

Table A7: Discard Rate, Dynamical score, Physical Invariance score, and Conservation metrics for Projectile

Experiment Name	Categories	Prompt Type	Discard Rate(\downarrow)	Dynamical Score(\uparrow)	Physical Invariance Score(\uparrow)	Energy Conservation(\uparrow)	Period Conservation(\uparrow)	Distance Conservation(\uparrow)
real-world	real-world video	-	0.000	0.98	0.939	0.999	0.882	0.936
COSMOS	single-frame	enhanced	0.370	0.51	0.484	0.477	0.443	0.531
COSMOS	single-frame	plain	0.250	0.54	0.481	0.607	0.531	0.305
CogVideo	single-frame	enhanced	0.141	0.35	0.545	0.539	0.331	0.765
CogVideo	single-frame	plain	0.400	0.43	0.352	0.279	0.312	0.464
LTX	single-frame	enhanced	0.920	0.05	0.065	0.072	0.047	0.076
LTX	single-frame	plain	0.560	0.26	0.348	0.407	0.223	0.414
PyramidalFlow	single-frame	enhanced	0.340	0.43	0.523	0.405	0.579	0.585
PyramidalFlow	single-frame	plain	0.235	0.45	0.408	0.617	0.315	0.290
COSMOS	multi-frame	enhanced	0.170	0.67	0.703	0.614	0.691	0.802
COSMOS	multi-frame	plain	0.374	0.47	0.535	0.475	0.524	0.604
CogVideo	multi-frame	enhanced	0.070	0.37	0.585	0.368	0.577	0.811
CogVideo	multi-frame	plain	0.140	0.53	0.528	0.388	0.508	0.688
LTX	multi-frame	enhanced	0.140	0.50	0.619	0.584	0.509	0.763
LTX	multi-frame	plain	0.240	0.52	0.599	0.537	0.595	0.663
PyramidalFlow	multi-frame	enhanced	0.130	0.46	0.686	0.555	0.718	0.785
PyramidalFlow	multi-frame	plain	0.130	0.45	0.548	0.702	0.517	0.424
CogVideo	first&last frame	enhanced	0.000	0.85	0.634	0.553	0.555	0.793
CogVideo	first&last frame	plain	0.030	0.85	0.660	0.613	0.604	0.763

Table A8: Discard Rate, Dynamical score, Physical Invariance score, and Conservation metrics for Holonomic Pendulum

Experiment Name	Categories	Prompt Type	Discard Rate(\downarrow)	Dynamical Score(\uparrow)	Physical Invariance Score(\uparrow)
real-world	real-world video	-	0.000	0.98	0.996
COSMOS	single-frame	enhanced	0.378	0.45	0.537
COSMOS	single-frame	plain	0.245	0.54	0.687
CogVideo	single-frame	enhanced	0.101	0.83	0.452
CogVideo	single-frame	plain	0.061	0.86	0.485
LTX	single-frame	enhanced	0.720	0.15	0.233
LTX	single-frame	plain	0.390	0.40	0.504
PyramidalFlow	single-frame	enhanced	0.330	0.52	0.512
PyramidalFlow	single-frame	plain	0.300	0.51	0.480
COSMOS	multi-frame	enhanced	0.364	0.45	0.594
COSMOS	multi-frame	plain	0.356	0.46	0.609
CogVideo	multi-frame	enhanced	0.040	0.80	0.503
CogVideo	multi-frame	plain	0.030	0.80	0.495
LTX	multi-frame	enhanced	0.130	0.62	0.685
LTX	multi-frame	plain	0.140	0.58	0.652
PyramidalFlow	multi-frame	enhanced	0.500	0.34	0.446
PyramidalFlow	multi-frame	plain	0.480	0.33	0.466
CogVideo	first&last frame	enhanced	0.230	0.71	0.448
CogVideo	first&last frame	plain	0.160	0.77	0.503

Table A9: Discard Rate, Dynamical score and Physical Invariance score for Non-nolonomic Pendulum

G Impact statement

Advancing physics-aware generative models is crucial for bridging perception and reasoning in AI, enabling more reliable simulations for robotics, scientific discovery, and autonomous systems. This paper introduces MORPHEUS, a benchmark revealing significant physical violations in video generation models, highlighting the need for integrating physics constraints into generative AI.

Experiment Name	Categories	Prompt Type	Discard Rate(\downarrow)	Dynamical Score(\uparrow)	Physical Invariance Score(\uparrow)
real-world	real-world video	-	0.000	0.99	0.938
COSMOS	single-frame	enhanced	0.103	0.86	0.555
COSMOS	single-frame	plain	0.086	0.86	0.538
CogVideo	single-frame	enhanced	0.047	0.90	0.578
CogVideo	single-frame	plain	0.000	0.93	0.537
LTX	single-frame	enhanced	0.778	0.21	0.152
LTX	single-frame	plain	0.337	0.64	0.448
PyramidalFlow	single-frame	enhanced	0.207	0.77	0.463
PyramidalFlow	single-frame	plain	0.154	0.81	0.511
COSMOS	multi-frame	enhanced	0.101	0.88	0.547
COSMOS	multi-frame	plain	0.134	0.83	0.528
CogVideo	multi-frame	enhanced	0.060	0.88	0.526
CogVideo	multi-frame	plain	0.000	0.91	0.566
LTX	multi-frame	enhanced	0.059	0.91	0.617
LTX	multi-frame	plain	0.015	0.94	0.604
PyramidalFlow	multi-frame	enhanced	0.149	0.84	0.565
PyramidalFlow	multi-frame	plain	0.152	0.83	0.551

Table A10: Discard Rate, Dynamical score and Physical Invariance score for Double Pendulum